AD-A084 238 AERONAUTICAL RESEARCH ASSOCIATES OF PRINCETON INC NJ F/G 20/4
FUNDAMENTAL RESEARCH IN TURBULENT MODELING.(U)
FEB 80 C CERASOLI, C DUP. DONALDSON, G SANDRI F44620-76-C-0048
UNCLASSIFIED ARAP-TM-80-2 AFOSR-TR-80-0324 NL

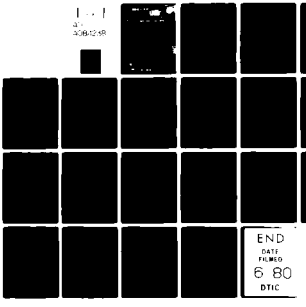

END
DATE FILMED
6 80
DTIC

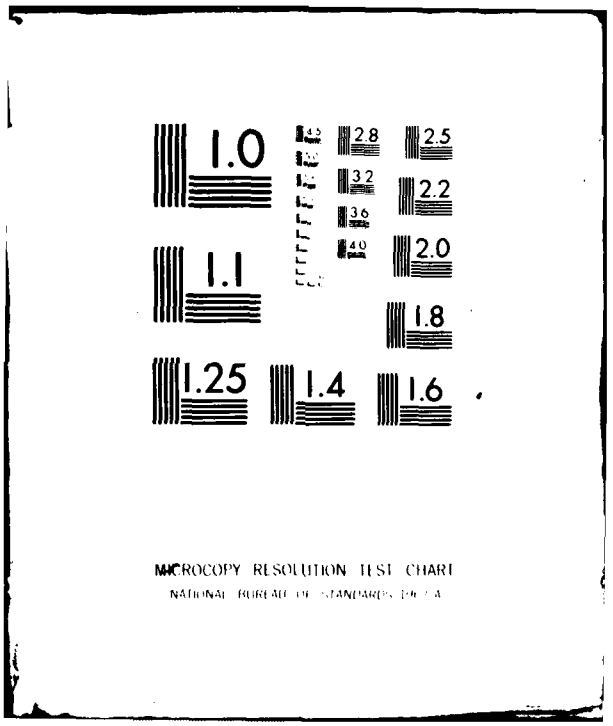
1.0
1.1
1.25
1.4
1.6
1.8
2.0
2.2
2.5
2.8
3.2
3.6
4.0
MICROCOPY RESOLUTION TEST CHART
NATIONAL BUREAU OF STANDARDS-1963-A

UNCLASSIFIED

SECURITY CLASSIFICATION OF THIS PAGE (When Data Entered)

(19) REPORT DOCUMENTATION PAGE	READ INSTRUCTIONS BEFORE COMPLETING FORM
(18) 1. REPORT NUMBER: AFOSR-TR-80-0324	2. GOVT ACCESSION NO.: AD-A084238
	3. RECIPIENT'S CATALOG NUMBER
(6) 4. TITLE (and Subtitle): FUNDAMENTAL RESEARCH IN TURBULENT MODELING.	(9) 5. TYPE OF REPORT & PERIOD COVERED: Technical Annual report. 1 Jan [illegible] – 31 Dec 1979
	6. PERFORMING ORG. REPORT NUMBER: ARAP Tech Memo 80-2
(10) 7. AUTHOR(s): CARMEN CERASOLI, COLEMAN duP DONALDSON, GUIDO SANDRI	(15) 8. CONTRACT OR GRANT NUMBER(s): F44620-76-C-0048
9. PERFORMING ORGANIZATION NAME AND ADDRESS: AERONAUTICAL RESEARCH ASSOCIATES OF PRINCETON, INC. 50 WASHINGTON ROAD PRINCETON, NEW JERSEY 08540	(16) 10. PROGRAM ELEMENT, PROJECT, TASK AREA & WORK UNIT NUMBERS: 2307A2 (17) 61102F
11. CONTROLLING OFFICE NAME AND ADDRESS: AIR FORCE OFFICE OF SCIENTIFIC RESEARCH/NA BLDG 410 BOLLING AIR FORCE BASE, D C 20332	(11) 12. REPORT DATE: Feb[illegible]80
	13. NUMBER OF PAGES: 42
14. MONITORING AGENCY NAME & ADDRESS (if different from Controlling Office) (12) 42	15. SECURITY CLASS. (of this report): Unclassified
(14) ARAP-TM-80-2	15a. DECLASSIFICATION/DOWNGRADING SCHEDULE

16. DISTRIBUTION STATEMENT (of this Report)

Approved for public release; distribution unlimited.

17. DISTRIBUTION STATEMENT (of the abstract entered in Block 20, if different from Report)

18. SUPPLEMENTARY NOTES

19. KEY WORDS (Continue on reverse side if necessary and identify by block number)

TURBULENCE
SCALE EQUATIONS
SECOND-ORDER CLOSURE
CORRELATION FUNCTIONS
TWO-POINT CORRELATION TENSORS

20. ABSTRACT (Continue on reverse side if necessary and identify by block number)

A summary of both the theoretical and experimental studies carried out during the first year of a program of fundamental research on turbulent modeling is given. On the theoretical side, the application of a modeled tensor scale equation together with a modeled Reynolds stress equation to the case of homogeneous shear flow is discussed in some detail. It is shown that such modeling gives results that are in good agreement with experiment. On the experimental side, preliminary data on the effect of swirl on the structure of turbulence in an annular pipe flow are presented.

DD FORM 1 JAN 73 1473 EDITION OF 1 NOV 65 IS OBSOLETE UNCLASSIFIED 00940

TABLE OF CONTENTS

1. INTRODUCTION

In the last few years, second-order-closure methods have become increasingly popular as a means of computing turbulent shear flows. These methods differ from eddy viscosity methods in that local turbulent transport is not assumed to be dependent on local mean gradients in the flow but, depending on the complexity of the model used, is a function of the development of all the independent second-order turbulent correlations in the flow ($\overline{u_i'u_j'}$, $\overline{\rho u_i'}$, $\overline{\rho'^2}$, etc.) or some measure of these quantities ($\overline{u_i'u_i'} = q^2 = 2k$ and $\overline{T'^2}$, for example). In order to calculate the six components of $\overline{u_i'u_j'}$ or the turbulent energy $k = q^2/2$ which is then used to estimate the components of $\overline{u_i'u_j'}$, equations for $\overline{u_i'u_j'}$ or q^2 are required. To date, these equations have contained a scale parameter Λ for which, in the purportedly more general methods, an equation is devised by modeling. In some of the methods, the scale is measured by the dissipation ε which, at high Reynolds numbers, is proportional to q^3/Λ or $k^{3/2}/\Lambda$. In such methods, generally referred to as $k-\varepsilon$ methods, k is used as a measure of the components of $\overline{u_i'u_j'}$ and ε is used to measure the turbulent scale Λ . In other methods, called $q-\Lambda$ methods, q is used as a measure of $\overline{u_i'u_j'}$ and an equation for Λ is given explicitly. In more complicated models where equations for all the second-order correlations are used, it is still common practice to use an equation which defines a single turbulent integral scale at any point in the flow. The equation for this scale may either be an ε equation or an explicit equation for Λ .

That the single scale methods described above have given us much new insight into the development of certain turbulent flows that could not be computed accurately before is unquestioned. However, there are flows for which such simplification is not possible. Even for the flows for which such methods calculate to an acceptable degree of accuracy the main features of the flow, there are differences between computed results and actual

measurements that are disquieting. Furthermore, on logical or esthetic grounds, the authors of this report have always felt a certain discomfort. The logical argument against the scale equations popular today is that we know that the turbulent structures in all turbulent flows are not the same, yet we use the same equation to compute the scale (in essence, the structure) in all flows.

Prior to the start of the present contract, Drs. Sandri and Donaldson were able to show that the scale equations currently in use could not be invariant equations if the so-called "constants" used in these equations were indeed constants.

The work being performed under the present contract is an attempt to develop remedies for the shortcomings of present methods. Our effort takes two different routes, one theoretical and one experimental.

On the theoretical side, we have (a) tried to generalize existing methods for putting scales into second-order-closure calculations so that the equations used are invariant equations, and (b) tried to generalize the methods so that the experimentally observed fact that the scales of all correlations near a solid surface do not behave in an identical way. These two efforts will be discussed in more detail in Section 2.

On the experimental side, we have tried to perform an experiment in the laboratory that would allow one to see the effect of stability on changing the relative scales of different correlations in a turbulent flow. Some details of our experimental work to date will be given in Section 3.

In Section 4 we will attempt to summarize our work to date and explain its significance. Finally, in Section 5, we shall report briefly on meetings attended, papers presented or planned, and, in general, on our interaction with the scientific community.

2. THEORETICAL DEVELOPMENTS

General Considerations

We have obtained previously (Ref. 1) a rate equation for the tensor scale Λ_{ij} from models of the two-point correlation tensor R_{ij}

$$R_{ij}(\hat{x},\hat{y}) = \left\langle u_i'(\hat{x})u_j'(\hat{y})\right\rangle \quad , \quad R_{ij}(\hat{x},\hat{x}) = \overline{u_i'u_j'}(\hat{x}) \tag{1}$$

These models were designed to describe turbulent flows which are far from walls or surfaces of strong stability. We shall call these models "standard models." A code for Λ_{ij} has since been implemented both in A.R.A.P. codes and in a code delivered to NASA for its own studies of turbulent flow. The tensor scale is defined by

$$\Lambda_{ij}(\hat{x}_c) = \frac{1}{q^2/3}\int \frac{R_{ij}(\hat{x}_c,\hat{r})\ d\hat{r}}{4\pi r^2} \tag{2}$$

where $\hat{r} = \hat{y} - \hat{x}$ and $\hat{x}_c = \frac{1}{2}(\hat{x} + \hat{y})$. To obtain a differential equation for Λ_{ij} , we take three steps:

(I) Close the R_{ij} equation so that when $\hat{y} \to \hat{x}$ we obtain a standard $\overline{u_i'u_j'}$ equation .

(II) Substitute into the closed R_{ij} equation the moment expansion

$$R_{ij}(\hat{x}_c,\hat{r}) = M^0_{ij}4\pi r^2\delta(\hat{r}) - M^1_{ijk}4\pi r^2\frac{\partial}{\partial r_k}\delta(\hat{r}) + \ldots \tag{3}$$

We note that by integrating over all $\hat{r}$, one finds

$$M^0_{ij} = \frac{q^2}{3}\Lambda_{ij} \tag{4}$$

(III) Integrate term by term over all $\hat{r}$. A simple choice of R_{ij} models yields

---

1. Sandri, G.: A New Approach to the Development of Scale Equations for Turbulent Flows. A.R.A.P. Report No. 302, April 1977.

$$\frac{\partial}{\partial t}\left(q^2\Lambda_{ij}\right) + \bar{u}_k \frac{\partial}{\partial x_k}\left(q^2\Lambda_{ij}\right) + q^2\left(\Lambda_{ik}\frac{\partial \bar{u}_j}{\partial x_k} + \Lambda_{jk}\frac{\partial \bar{u}_i}{\partial x_k}\right) =$$

$$= v_{c_1}\frac{\partial}{\partial x_k}\left[(q\Lambda)\frac{\partial}{\partial x_k}\left(q^2\Lambda_{ij}\right)\right] + v_{c_2}\frac{q^2}{\Lambda}\Lambda_{ij} +$$

$$- \frac{q^3}{\Lambda}\left(\Lambda_{ij} - \delta_{ij}\frac{\Lambda_{kk}}{3}\right) - \frac{2}{3}bq^3\delta_{ij} \qquad (5)$$

where Λ is the single scale utilized in the standard model and in the universal scale equation. We identify Λ as follows:

$$\Lambda = \frac{1}{3}\Lambda_{kk} \qquad (6)$$

because for locally isotropic turbulence, $\Lambda = \frac{2}{3}L_f$ where L_f is the Taylor longitudinal scale, a relation supported by analysis of a number of flows. Taking the trace of Eq. (5) and subtracting the equation for q^2, we find the rate equation for Λ, namely,

$$\frac{\partial \Lambda}{\partial t} + \bar{u}_k \frac{\partial}{\partial x_k}\Lambda + \underline{2\Lambda\left(\frac{\Lambda_{ij}}{3\Lambda} - \frac{\overline{u_i'u_j'}}{q^2}\right)\frac{\partial \bar{u}_i}{\partial x_j}} =$$

$$= \frac{v_{c_1}}{q}\left\{\frac{\partial}{\partial x_k}\left[q\Lambda\frac{\partial}{\partial x_k}(q^2\Lambda)\right] - \Lambda\frac{\partial}{\partial x_k}\left[q\Lambda\frac{\partial q^2}{\partial x_k}\right]\right\} +$$

$$+ \left(\frac{4}{3}b + v_{c_2}\right)q \qquad (7)$$

We note that the coefficient of the production term (which is underlined in the above equation) depends on the flow structure rather than being a constant as in the universal scale model.

To obtain the (approximate) relation between the trace of the tensor scale equation and the universal Λ equation, we decompose the tensor Λ_{ij} into its trace and the traceless deviatoric part Δ_{ij}

$$\Lambda_{ij} = \frac{1}{3}\Lambda_{kk}\delta_{ij} + \Delta_{ij} \tag{8}$$

We then obtain an equation for Δ_{ij} by substitution of Eq. (8) into (5):

$$\frac{\partial}{\partial t}\left(q^2\Delta_{ij}\right) + \bar{u}_k \frac{\partial}{\partial x_k}\left(q^2\Delta_{ij}\right) + q^2\left(\Delta_{ik}\frac{\partial \bar{u}_j}{\partial x_k} + \frac{\partial \bar{u}_i}{\partial x_k}\Delta_{kj}\right) +$$

$$- \frac{2}{3}\delta_{ij}q^2\Delta_{\alpha k}\frac{\partial \bar{u}_\alpha}{\partial x_k} = - q^2\Lambda\left(\frac{\partial \bar{u}_i}{\partial x_j} + \frac{\partial \bar{u}_j}{\partial x_i}\right) +$$

$$+ v_c \frac{\partial}{\partial x_k}\left[q\Lambda \frac{\partial}{\partial x_k}\left(q^2\Delta_{ij}\right)\right] - \left(1 - v_{c_2}\right)\frac{q^3}{\Lambda}\Delta_{ij} \tag{9}$$

A first approximation to Eq. (9) is obtained by introducing an "anisotropy parameter" σ defined by

$$\Delta_{ij} = \sigma\Lambda\left(\frac{\overline{u_i'u_j'}}{q^2} - \frac{\delta_{ij}}{3}\right) \tag{10}$$

Substitution of Eq. (10) into (9) yields (Ref. 2)

$$\frac{\partial \sigma}{\partial t} + \bar{u}_k \frac{\partial}{\partial x_k}\sigma - 2\left(\frac{\sigma}{3} - 1\right)\left(\sigma + \frac{q^4}{\overline{u_i'u_j'}\ \overline{u_i'u_j'} - \frac{q^4}{3}}\right)\overline{u_m'u_n'}\frac{\partial \bar{u}_m}{\partial x_n} =$$

$$= \frac{v_{c_1}}{\Lambda}\left\{\frac{\partial}{\partial x_k}\left[q\Lambda\frac{\partial}{\partial x_k}(\sigma\Lambda)\right] - \sigma\frac{\partial}{\partial x_k}\left[q\Lambda\frac{\partial \Lambda}{\partial x_k}\right]\right\} +$$

$$- \sigma\left(\frac{2}{3} + \frac{v_{c_2}}{b}\right)\frac{2bq}{\Lambda} \tag{11}$$

In the universal scale equation, the "constant" which scales the production term in the equation is generally taken to be approximately 0.35. Thus, if we set

---

2. Sandri, G.: Recent Results Obtained in the Modeling of Turbulent Flows by Second-Order Closure. AFOSR-TR-78-0680, February 1978.

$$-2\left(\frac{\sigma}{3} - 1\right) = 0.35 \qquad (12)$$

we find that this choice corresponds to $\sigma = 2.5$. The super-equilibrium solution of Eq. (11) for plane shear flows gives $\sigma = 2.7$ which is in good agreement with Eq. (12). For this approximation, we find, after substituting Eqs.(10) and (12) into (8)

$$\frac{\Lambda_{11}}{\Lambda} = 1.4 \quad , \quad \frac{\Lambda_{22}}{\Lambda} = \frac{\Lambda_{33}}{\Lambda} = 0.8 \quad , \quad \frac{\Lambda_{12}}{\Lambda} = \frac{\Lambda_{21}}{\Lambda} = -0.5 \qquad (13)$$

Note that Λ_{12} is not a length but the (angular-averaged) integral scale of the correlation component $\left\langle u_1'(\hat{x}) u_2'(\hat{y}) \right\rangle$ which is typically negative in plane shear flows. A marked advantage of the method described above to obtain an approximate solution for Λ_{ij} lies in the fact that the trace part of Λ_{ij} is not forced to equilibrium. This feature is essential if agreement with the extensive experiments carried out at Johns Hopkins (Ref. 3) on homogeneous shear turbulence is to be obtained, because in these experiments Λ (and q^2) grow indefinitely. We obtained a strong test of our model by comparing an exact solution of the coupled $\overline{u_i' u_j'}$ and Λ_{ij} equations for homogeneous shear with the Johns Hopkins data. We write the velocity field as $\left(U(y),0,0\right)$ and substitute into the $\overline{u_i' u_j'}$ equation and into Eq. (5) the forms

$$\overline{u_i' u_j'} = U_{ij}\, e^{+2aU't} \quad , \quad \Lambda_{ij} = L_{ij}\, e^{+aU't} \qquad (14)$$

The factor of 2 in the growth rate of the Reynolds tensor is due to its quadratic nature.

It is most interesting that the forms (Eq. (14)) result in a cancellation of the exponentials in spite of the nonlinearity

---

3. Harris, V.G., Graham, J.A.H., and Corrsin, S.: Further Experiments in Nearly Homogeneous Turbulent Shear Flow. J. Fluid Mech. 81, 1977, pp. 657-688.

of the equations, and the tensor equations become algebraic and can be solved explicitly. We find, in particular, the following expressions for the Bradshaw number B, the Corrsin parameter C, the ratio of turbulent to shear time scales $1/\alpha$, and the growth rate a contained in Eq. (14)

$$B = \frac{|\overline{u_1' u_2'}|}{q^2} = \frac{1}{1 + 2v_{c_2}} \sqrt{\frac{(1 - 2b)(b + v_{c_2})}{3}} \tag{15}$$

$$C = \frac{|\overline{u_1' u_2'}|}{\left(\overline{u_1'^2}\ \overline{u_2'^2}\right)^{\frac{1}{2}}} = \sqrt{\frac{3(b + v_{c_2})}{1 + 4b + 6v_{c_2}}} \tag{16}$$

$$\frac{1}{\alpha} = \frac{q}{U'\Lambda} = \frac{1}{1 + 2v_{c_2}} \sqrt{\frac{1 - 2b}{3(b + v_{c_2})}} \tag{17}$$

$$a = v_{c_2} \frac{1}{\alpha} = \frac{v_{c_2}}{1 + 2v_{c_2}} \sqrt{\frac{1 - 2b}{3(b + v_{c_2})}} \tag{18}$$

A good fit to the energy and scale behavior of grid turbulence, analyzed as if perfectly isotropic, gives $v_{c_2} = 0.07$, $b = 0.125$ implying

$$C = 0.5 \quad , \quad B = 0.18 \tag{19}$$

C is in excellent agreement with experiment. The growth rate also compares well with the data. The model further predicts

$$\frac{\Lambda_{11}}{\Lambda_{22}} = 2.5 \quad , \quad \frac{|\Lambda_{12}|}{3\Lambda} = 0.19 \tag{20}$$

which could eventually be checked. These values are in rough agreement with the σ approximation, Eq. (13).

From several computer integrations of the coupled Λ_{ij} and $\overline{u_i' u_j'}$ which were carried out with a wide variation in initial conditions, it appears that our solution, Eqs. (14) - (18), is

a "convective superequilibrium" which represents the asymptotic long-time solution. The ratio α is close to one for the best experimental runs as well as from Eq. (17), suggesting that fine-tuning the experimental initial conditions would lead to a more rapid onset of the asymptotic state than was measured experimentally and thus would enhance the amount of experimental data that could be used to check our theory. The qualitative physical picture that emerges for homogeneous shear flows is as follows: (a) during the initial transient, if $q_o/\Lambda_o \ll U'$, the shear brings the turbulence by "sudden distortion" up to convective equilibrium ($q/\Lambda \approx U'$); (b) if $q_o/\Lambda_o \gg U'$, the turbulence decays in a "grid"-like manner to the convective equilibrium ($q/\Lambda \approx U'$). There, a merging mechanism takes over (a multi-layer Brown-Roshko effect) so that eddies fold with each other, making larger ones indefinitely (i.e., as long as the imposed shear provides the energy to sustain the process). Once the merging process takes over, the eddy structure remains fixed and exhibits highly directional integral scales (Eq. (20)).

A further test of our modeling consists in directly compaing the structure predicted by the R_{ij} model with experimental data. The simplest flow on which detailed structural information (Energy Spectra) is available is grid turbulence. A first cut at the analysis can be made by assuming that grid turbulence is isotropic. This assumption is in fact not correct, and a more general framework is needed in order to understand the full details of the measured spectra. A remarkable result can be demonstrated, however. For high turbulence Reynolds numbers ($q\Lambda/\nu$ large), the energy dissipation is given experimentally by

$$\frac{\partial q^2}{\partial t} = - 2b \frac{q^3}{\Lambda} \quad , \qquad b \approx 0.125 \tag{21}$$

A theorem due to G.I. Taylor (Ref. 4) states on the other hand

---

4. Batchelor, G.K.: *The Theory of Homogeneous Turbulence*, Cambridge University Press, 1953, p. 100.

$$\frac{\partial q^2}{\partial t} = - 2\nu \frac{q^2}{\lambda^2} \tag{22}$$

The two statements of dissipation are equivalent if the following relation (Glushko (Ref. 5)) is assumed

$$\lambda^2 = \frac{\Lambda^2}{a + b \frac{q\Lambda}{\nu}} \tag{23}$$

We demonstrate below that a simple model of cascading (needed to obtain closure of the R_{ij} equation) implies (23). We introduce wave number space by

$$\Phi_{ij}(\vec{k}) = \frac{1}{8\pi^3} \int R_{ij}(\vec{r})\ e^{-i\vec{k}\cdot\vec{r}}\ d\vec{r} \tag{24}$$

and the three-dimensional spectrum, E , by the Karman-Howarth relation

$$\Phi_{ij}(\vec{k}) = \left(\delta_{ij} - \frac{k_i k_j}{k^2}\right) \frac{E(k)}{4\pi k^2} \tag{25}$$

The normalization is chosen so that

$$\frac{q^2}{2} = \int_0^\infty E(k)\ dk \tag{26}$$

The R_{ij} equation becomes

$$\frac{\partial E}{\partial t} = T(k) - 2\nu k^2 E \tag{27}$$

where the transfer function T which represents cascading (more properly, in our view, eddy size rearrangement) satisfies

$$\int_0^\infty T(k)\ dk = 0 \tag{28}$$

i.e., eddy size rearrangement does not change the energy. A

---

5. Glushko, G.S.: Turbulent Boundary Layer on a Flat Plate in an Incompressible Fluid. Bull. Acad. Sciences, USSR, Mech. Series No. 4, 1965, pp. 13-23.

simple model for T, which has derivatives only (no integrals*) both in $\vec{k}$ space and for R_{ij}, is

$$T = -\frac{q}{\Lambda}\alpha\left[\frac{5}{3}E + k\frac{\partial E}{\partial k}\right] + \frac{2}{3}\frac{q}{\Lambda}\alpha\lambda^2k^2E \tag{29}$$

The coefficients have been chosen so that for Kolmogoroff equilibrium, i.e., $T = 0$, the only solution is

$$E = \text{const} \cdot k^{-5/3}$$

and, in addition, Eq. (28) is satisfied. To obtain Eq. (23), we consider a steady source at k_o

$$\frac{q}{\Lambda}\alpha\left[\frac{5}{3}E + k\frac{\partial E}{\partial k}\right] + 2\nu k^2E\left[\frac{\alpha}{3}\text{Re}\frac{\lambda^2}{\Lambda^2} - 1\right] =$$

$$= Q_o\delta(k - k_o), \quad \text{Re} \equiv \frac{q\Lambda}{\nu} \tag{30}$$

The exact solution is

$$E = \frac{Q_o}{\frac{q}{\Lambda}\alpha k_o}e^{\kappa}H\left(\frac{k}{k_o} - 1\right)\frac{e^{-(k/k_o)^2\kappa}}{(k/k)^{5/3}} \tag{31}$$

with H the Heaviside function and

$$\kappa = \frac{k_o^2\Lambda^2}{\alpha\text{Re}} - \frac{k_o^2\lambda^2}{3} \tag{32}$$

We now impose, as integral constrains, the definitions of $q^2/2$, λ, and Λ.

---

* For purposes of calculational feasibility, it is most desirable that the model equations be differential. If both ϕ_{ij} and R_{ij} are to be governed by differential equations, then all terms in the modeling of T must be of the form $a_nk^n\partial^nE/\partial k^n$. A general consequence of such assumptions is that $\phi(k)$ will exhibit a region where ϕ is proportional to a power of k.

$$\frac{q^2}{2} = \int_0^\infty E(k)\, dk = E_o k_o I_1(\kappa) \tag{33}$$

$$\frac{q^2}{2}\,\frac{1}{\lambda^2} = \int_0^\infty k^2 E\, dk = E_o k_o^3 I_2(\kappa) \tag{34}$$

$$\frac{2}{\pi}\,\frac{q^2}{2}\,\Lambda = \int_0^\infty \frac{E}{k}\, dk = E_o I_3(\kappa) \tag{35}$$

where we have introduced three convenient integrals, I_1 , I_2 , and I_3 , and the abbreviation

$$E_o = \frac{Q_o}{(q/\Lambda)\alpha k_o}\, e^{\kappa} \tag{36}$$

After some manipulation, we find

$$\frac{\Lambda^2}{\lambda^2} = \frac{e^{-\kappa}}{2I_1(\kappa)}\, \alpha Re \tag{37}$$

Numerical evaluation of I_1 then gives

$$\lambda^2 \approx \frac{\Lambda^2}{\frac{\pi^2}{4} + \frac{\alpha}{3} Re} \tag{38}$$

Comparing Eq. (38) with (23), we obtain

$$a = \frac{\pi^2}{4} = 2.47 \quad , \quad b = \frac{\alpha}{3} \tag{39}$$

It is interesting to note that the empirically accepted values of a lie between 3.25 and 2.5. We note here a general result, namely that a model of the eddy size rearrangement term in the R_{ij} equation determines the asymptotic model in the $\overline{u_i' u_j'}$ equation. This is not obvious when one merely considers the

contraction of the R_{ij} equation into the $\overline{u_i' u_j'}$ equation. From dimensional arguments, it can be shown that a family of models should yield the Glushko relation and, in addition, that if the spectrum has the Kolmogoroff form

$$E \underset{Re \to \infty}{\longrightarrow} A \varepsilon^{2/3} k^{-5/3} \qquad \text{for} \quad k > k_o \tag{40}$$

then the dissipation parameter b is given by

$$b = \frac{\pi}{5 \cdot 3^{3/2}} A^{-3/2} = 0.121 \, A^{-3/2} \tag{41}$$

Experimentally, $A \approx 1$; thus, Eq. (41) yields a value for b that is close to the generally accepted value of b , i.e., 0.125 .

The derivation of the scale equation, the agreement of the model with homogeneous shear flows, and the derivation of the Glushko relation are, in our opinion, strong arguments in support of developing a full model for R_{ij} .

Boundary Conditions on Pressure Fluctuations

An essential feature of second-order closure is that all terms that contain pressure fluctuations are expressed in terms of velocity fluctuations. It is therefore impossible to prescribe boundary conditions on the pressure fluctuations once the equations are closed. It is thus to be expected that, to calculate the details of certain flows near walls or regions of strong stability, models which use a single large scale Λ will require generalization. We have chosen the extreme case of atmospheric free convection as a flow suitable for investigating such generalizations because such flows exhibit strong disparities of scale (the strongest known to us) both in laboratory and atmospheric experiments. Furthermore, the wealth of experimental data that have been accumulated over the years gives a firm basis

for comparing models with observations. The most striking feature of the data is the fact that, while several variables scale very well with the Monin-Obukhov length parameter L

$$L \equiv - \frac{T_o}{\kappa g} \frac{u_*^3}{\overline{w'T'}} \quad , \quad u_*^2 = \left|\overline{u'w'}\right| \quad , \tag{42}$$

the horizontal variance scales only with the much larger length z_i , the mixing layer height. In (42) we have used the mean temperature of the surface layer T_o , the gravitational constant g , and von Kárman's constant κ ($\approx .39$). We generalize the standard Reynolds stress model by introducing, in addition to the scale $\Lambda = \frac{1}{3} \Lambda_{kk}$, a vertical scale Λ_v which we identify as

$$\Lambda_v = \text{const } \hat{g}_i \Lambda_{ij} \hat{g}_j \tag{43}$$

We impose the requirement that the generalized model should reduce to the standard one when $\Lambda - \Lambda_v \to 0$ because empirically the difference $\Lambda - \Lambda_v$ is an inverse measure of height above the ground. We have considered several alternative models and concluded that the most satisfactory fit to the data can be described by the following models:

1. For the pressure-rate of strain correlation, we add to the tendency-towards-isotropy term generally used a "pancaking"term

$$\left\langle p' \left(\frac{\partial u_i'}{\partial x_j} + \frac{\partial u_j'}{\partial x_i} \right) \right\rangle = - \frac{q}{\Lambda} F_p \left(\overline{u_i' u_j'} - \frac{q^2}{3} \delta_{ij} \right) +$$

$$- \frac{q}{\Lambda} F_p 3 \left(\frac{q^2}{3} - D \hat{g}_i \overline{w_i' w_j'} \hat{g}_j \right) \left[\hat{g}_i \hat{g}_j - \frac{1}{2} \left(\delta_{ij} - \hat{g}_i \hat{g}_j \right) \right] \tag{44}$$

where $\hat{g}_i$ is the unit vector normal to the ground and D is a free parameter. F_p is defined as

$$F_p = 1 - \zeta + c_1 \zeta \frac{\Lambda}{\Lambda_v} \frac{1}{q} \left(\hat{g}_i \overline{w_i' w_j'} \hat{g}_j \right)^{\frac{1}{2}} \tag{45}$$

We refer to this quantity Λ/qF_p as the eddy turnover time. In (45) we have introduced a tapering factor ζ which is given by

$$\zeta = 1 - \left(\Lambda_v/\Lambda\right)^{2/3} , \quad \zeta \xrightarrow[\Lambda_v \to \Lambda]{} 0 \tag{46}$$

2. The dissipation of the Reynolds tensor is assumed isotropic

$$- 2\nu \left\langle \frac{\partial u_i'}{\partial x_k} \frac{\partial u_j'}{\partial x_k} \right\rangle = - \frac{2bF_d}{\Lambda} \frac{\delta_{ij}}{3} q^3 \tag{47}$$

where the modifier of the dissipation time scale is

$$F_d = 1 - \zeta + c_2 \zeta \frac{\Lambda}{\Lambda_v} \frac{(\hat{g}_i \overline{w_i' w_j'} \hat{g}_j)^{3/2}}{q^3} \tag{48}$$

3. For the thermal equations, we adopt a parallel strategy. The two relevant models are the "pressure scrambling" of the heat flux

$$\left\langle T' \frac{\partial p'}{\partial x_i} \right\rangle = - \frac{Aq}{\Lambda} F_p \overline{u_i' T'} \tag{49}$$

and the dissipation of the temperature variance

$$-2k \left\langle \frac{\partial T'}{\partial x_i} \frac{\partial T'}{\partial x_i} \right\rangle = - \frac{2bs}{\Lambda} F_p \overline{T'^2} \tag{50}$$

We have not fully developed the tensor scale equation for the model, so that as a first approximation we prescribe the two scales within the surface layer as follows. For $L < 0$,

$$\Lambda = \frac{\alpha z}{(\alpha z/\varepsilon z_i) + e^{-(\gamma z/|L|)}} , \quad \Lambda_v = \alpha z \tag{51}$$

where $\alpha = .65(58992)$, $\varepsilon = .2$, $\gamma = 3$; while for $L > 0$ (stable side)

$$\Lambda = \min(\alpha z,\ .2z_i)\ ,\quad \Lambda_v = \min(\alpha z,\ .2L) \tag{52}$$

It will be noted that this modeling which was adopted after many analytical and numerical studies had been carried out adds four new parameters to the calculation of atmospheric flows. The parameters are $c_1 \approx 2$, $c_2 \approx 2$, $D \approx .58$, and $\gamma = 3$.

The results of the superequilibrium limit are gratifying. We have solved the rather intricate algebraic equations with a computer. We show in Figure 1 the behavior of $\sigma_H = (\overline{u'^2})^{\frac{1}{2}} = (\overline{v'^2})^{\frac{1}{2}}$; the scaling with z_i is clear and effectively independent of z ($z/L = -7$ was chosen). It is worth noting that we have obtained systematic improvements relative to the standard model on the vertical variance $(\overline{w'w'})^{\frac{1}{2}}$ (Figure 2), the horizontal heat flux $\overline{u'T'}$, and the temperature variance $\overline{T'^2}$. The behavior of

$$\phi \equiv + \frac{\kappa z}{u_*} \frac{\partial U}{\partial z} \qquad \text{and} \qquad \phi_h \equiv - \frac{\kappa z u_*}{\overline{w'T'}} \frac{\partial T}{\partial z} \tag{53}$$

remains essentially that given by the standard model. These results encourage our confidence in second-order closure in general for we have obtained substantial agreement comparing a second-order-closure model with experimental data on free convections which some individuals had considered unfeasible.

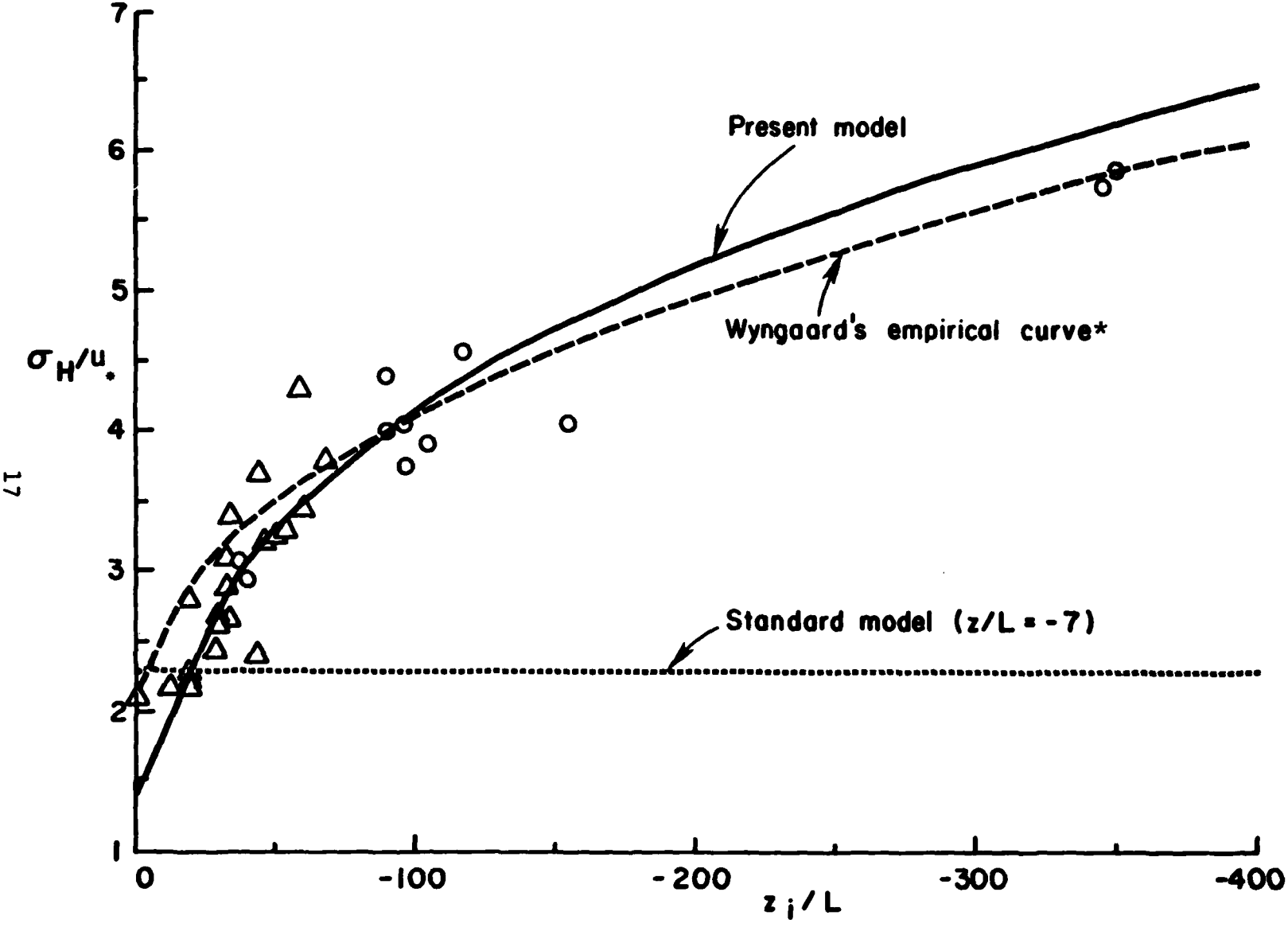

Figure 1.

* Wyngaard, J.C.: The Atmospheric Boundary Layer--Modeling and Measurements. Proc. 2nd Symp. on Turbulent Shear Flows, Imperial College, London, July 1979, pp. 13.25 - 13.30.

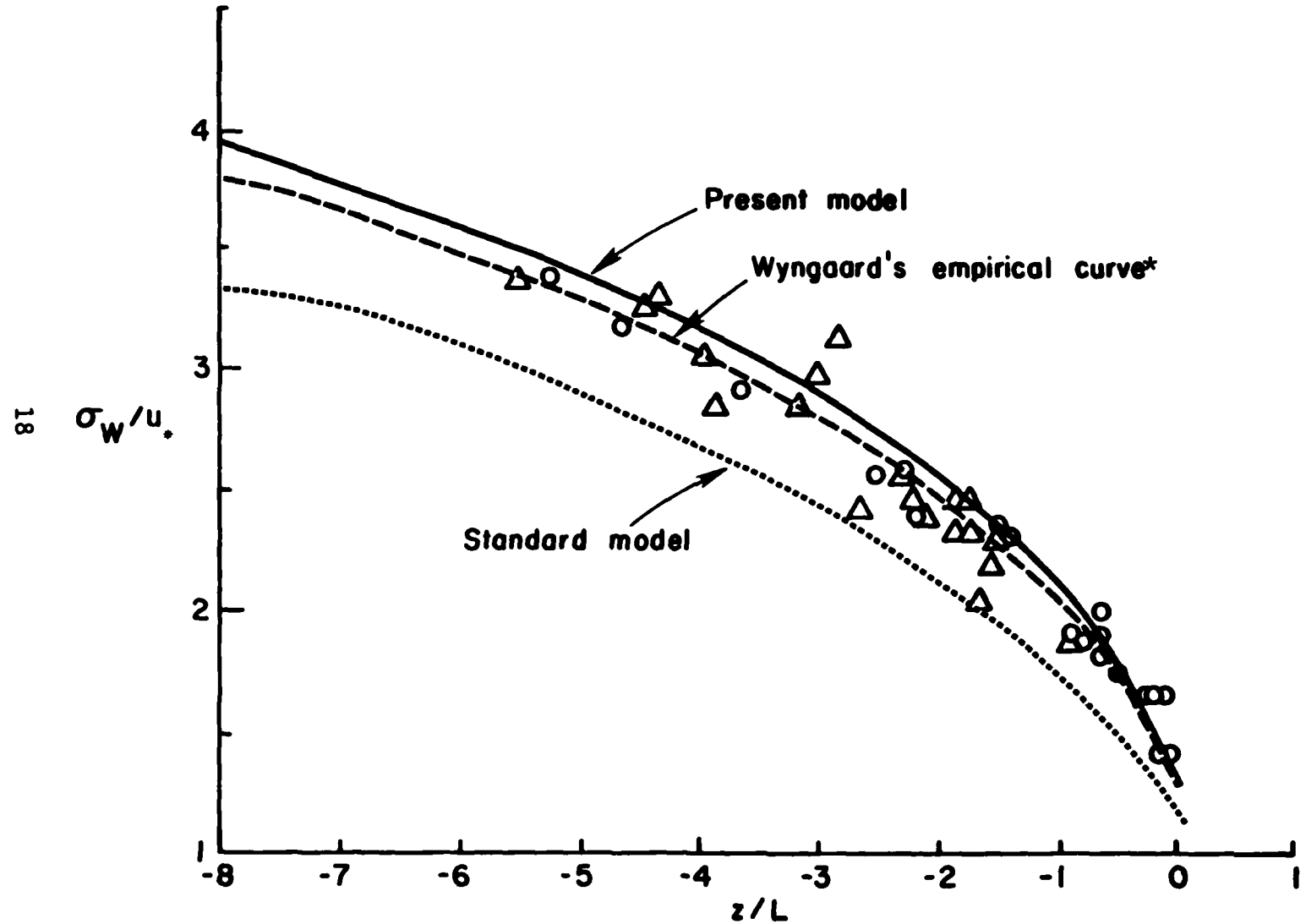

Figure 2.

*ibid

3. EXPERIMENTAL RESULTS

Apparatus

The vortex tube facility at A.R.A.P., in which we are trying to measure the effect of swirl on turbulent structure, will be briefly described. A more complete description can be found in a previous AFOSR technical report (Ref. 6). The test section has an annular cross section with inner and outer radii of 2.54 cm and 21.88 cm, respectively. The length of the tube can be varied by adding or subtracting sections, and the maximum downstream distance from the beginning of the tube proper is approximately 45 diameters. A schematic of the apparatus is shown in Figure 3. The inlet section, shown in Figure 4, allows swirl to be introduced by the setting of 32 equally spaced vanes. The flow then undergoes a contraction of about 25:1 and generates an approximate potential vortex flow (tangential velocity proportional to 1/radius).

The vortex tube facility has been upgraded in a number of ways. First, a system of hot wire probe supports was designed and fabricated which allow the measurement of two-point velocity correlations. At present, radial separations are possible, and a support system which will allow azimuthal separations is being designed. Second, the analog-to-digital data acquisition system is fully operational. Hot wire anemometer signals are transmitted from the vortex tube to the computer room via cable and then pass through a differential amplifier which removes all line noise. The A/D system allows data to be collected on up to 16 channels at a maximum sampling rate of 10^5 hz. Data taken with this system can be stored on tape to be analyzed later. A set of analysis programs has been written which allow the computation of power spectra, autocorrelations, single-point velocity correlations (Reynolds tensor components), and two-point

---

6. Bilanin, A.J., Snedeker, R.S. and Sullivan, R.D.: Experimental and Theoretical Study of Aircraft Vortices. AFOSR-TR-75-0664. February 1975.

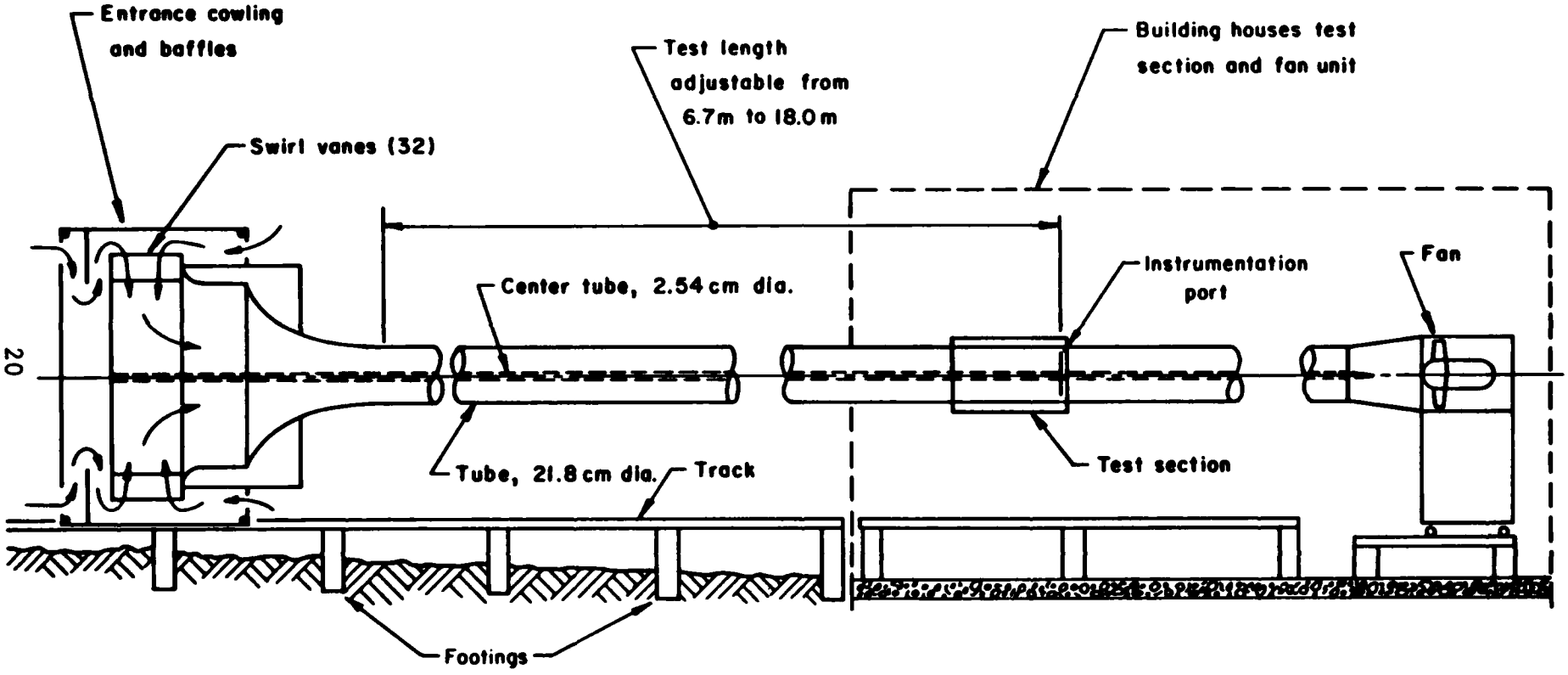

Figure 3. Schematic of A.R.A.P. vortex tube tunnel

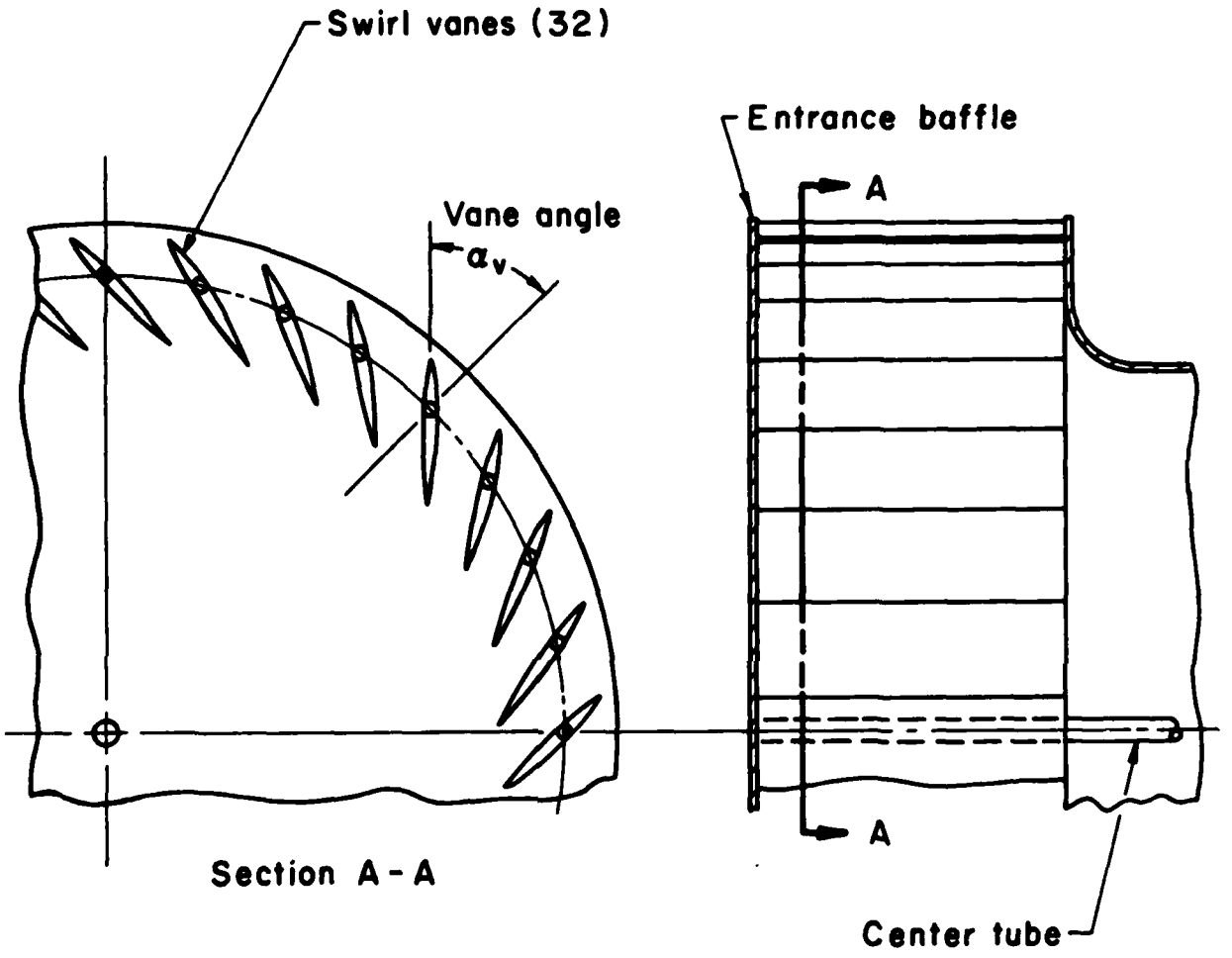

Figure 4. Detail of entrance section showing swirl vanes

correlations. The analysis program has been set up so that all the relevant statistics from a typical two-point correlation experiment can be computed overnight. Finally, modifications have been made to the vortex tube inlet section. Initial measurements showed that a great deal of unsteadiness existed in the flowfield. This was apparent in power spectra which exhibited a large amount of energy at very low frequencies (~ 0.1 hz to 1 hz). This unsteadiness was finally traced to nonuniformities in the inlet section and was remedied by placing a sheet of ½" polyurethane foam around the inlet section. This served to make the inflow more uniform and damp any large-scale motions. Further work will most likely be necessary on the inlet and contraction section to improve the vortex tube flow. Measurements for the no-swirl case show that the flow is not precisely symmetric about the centerline and differences of about 5% to 10% exist for the mean flow. In the case of high swirl flow, we have reason to believe azimuthally propagating disturbances are present. We suspect that these problems are associated with the contraction section, and design modifications are being considered.

Mean Velocities

A great deal of data has been collected for the no-swirl case, and we are beginning to generate a database for swirling flows. In the case of no-swirl flow, we have been able to compare our results to the literature on pipe flow. Mean velocity profiles for three vane angle settings are presented in Figure 5(a-c) where the downstream distance is approximately 30 diameters. Note that cylindrical coordinates are used so that $\bar{w}$ is the downstream velocity and $\bar{v}$ is the tangential velocity. (The radial flow $\bar{u}$ was too small to be accurately resolved.) The maximum value of $\bar{w}$ in all three cases was approximately 2500 cm/sec (~ 80 ft/sec) and all velocities were normalized by $\bar{w}_{max}$. The Reynolds number based on $\bar{w}_{max}$ and

the outer radius R_o was approximately 3.7×10^5 . (Note, we base Re on the radius rather than the diameter. This is because the presence of the central pipe limits the largest eddy to a size of R_o as opposed to $2R_o$.) The no-swirl case presented in Figure 5(a) shows a typical $\bar{w}(r)$ profile and a comparison of the profile in the outer region from $r/R_o = 0.55$ to 1.0 agrees well with pipe flow data at comparable Reynolds numbers (Refs. 7, 8). The case when the swirl vanes were set at twenty degrees ($\alpha_v = 20°$) is presented in Figure 5(b) and shows a $\bar{w}(r)$ profile which is substantially flatter than the no-swirl case. This can be attributed to increased mixing due to the presence of a tangential velocity and its associated deformation $\left(r \frac{d}{dr}\left(\frac{v}{r}\right)\right)$. The tangential velocity for this case is relatively week (~ 0.06 $\bar{w}_{max}$) and approximately constant as a function of radius. The $\alpha_v = 40°$ case, presented in Figure 5(c), shows a $\bar{w}(r)$ field similar to the previous case, while the $\bar{v}(r)$ field differs in magnitude and structure. In this case, $\bar{v}(r)$ is somewhat closer to a potential vortex in the region from $r/R_o = 0.30$ to $r/R_o = 0.60$, while an approximate rigid-body rotation region ($\bar{v} \propto r$) can be seen developing from $r/R_o = 0.70$ to $r/R_o = 0.95$.

A comparison between the present results and those obtained under our previous AFOSR contract (Ref. 6) show some interesting differences. In the previous work, $\bar{w}(r)$ profiles for the no-swirl case were much flatter than seen currently. Also, the $\bar{v}(r)$ field decayed more rapidly with downstream distance. The previous study showed the following behavior: $z/D \simeq 15$, $\bar{v} \sim 1/r$; $z/D \simeq 30$, $\bar{v} \sim$ constant ; $z/D \simeq 45$, $\bar{v} \sim r$. The present study shows that $\bar{v}$ is more like a potential vortex at

---

7. Schlichting, H.: *Boundary Layer Theory*, McGraw Hill, New York, 1968, pp. 560-564.

8. Laufer, J.: The Structure of Turbulence in Fully Developed Pipe Flows. National Advisory Committee for Aeronautics Report No. 1174, 1954.

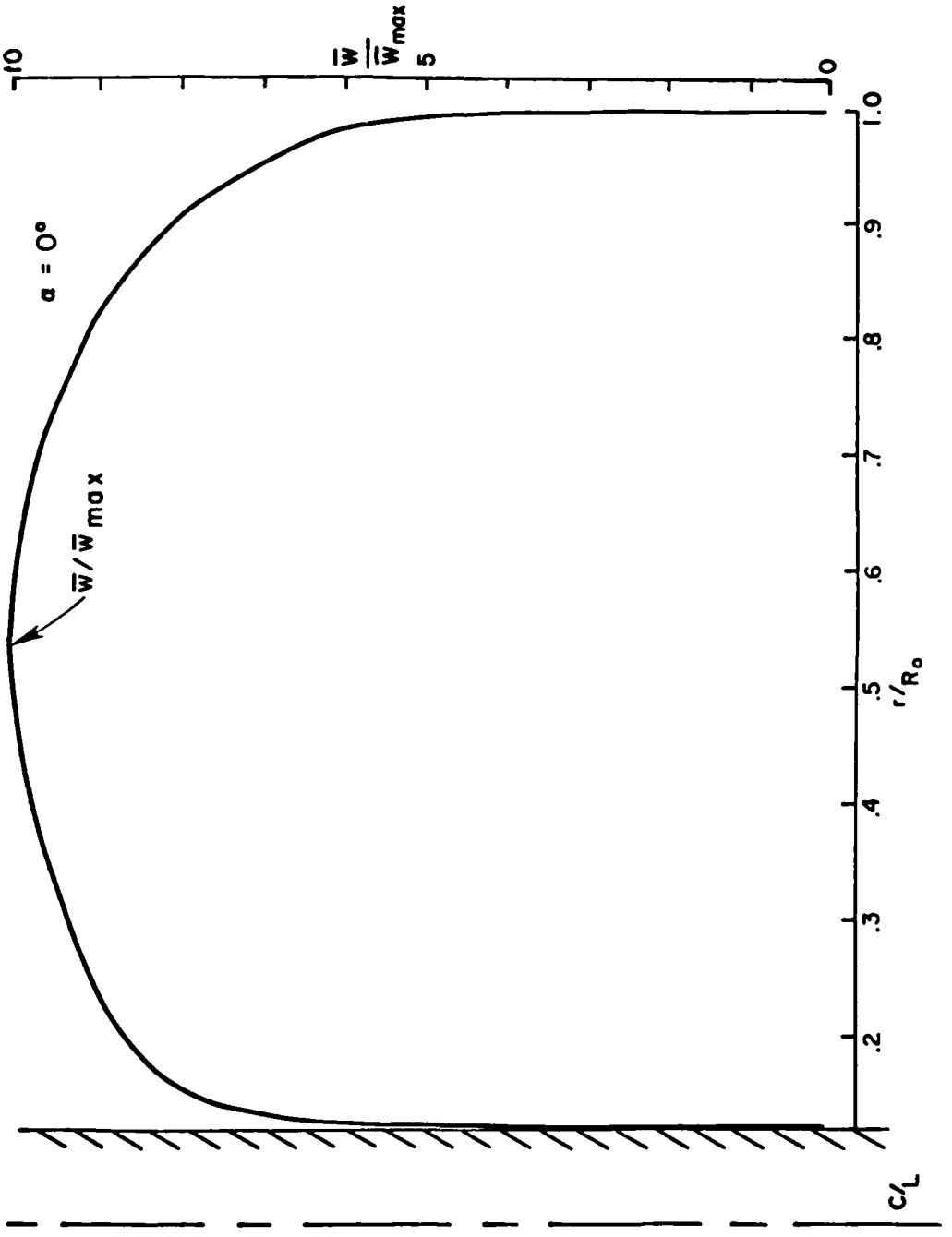

Figure 5(a).

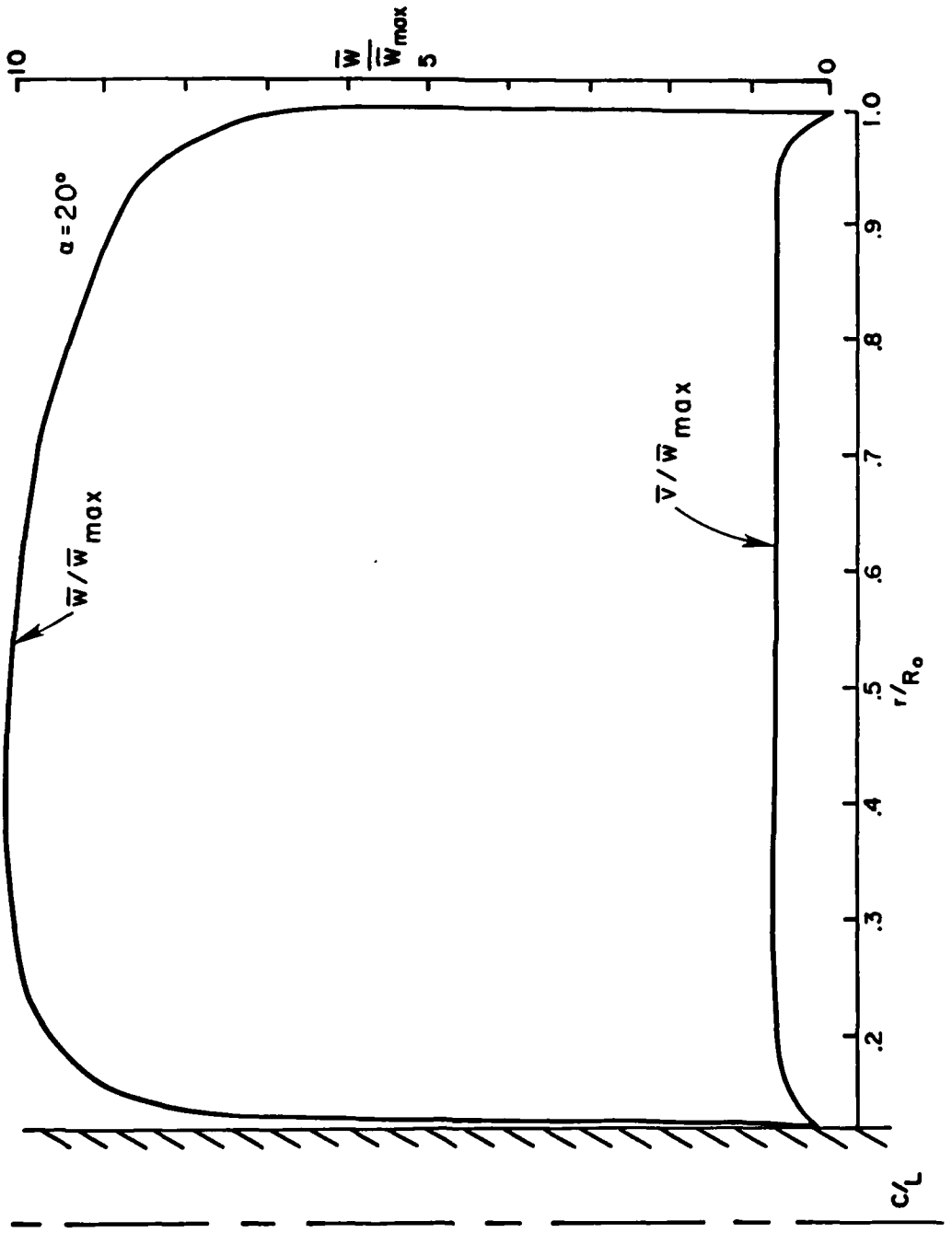
10
$\frac{\bar{w}}{\bar{w}_{max}}$
5
0
α=20°
$\bar{w}/\bar{w}_{max}$
$\bar{v}/\bar{w}_{max}$
1.0
.9
.8
.7
.6
.5
.4
.3
.2
r/R_o
C_L

Figure 5(b).

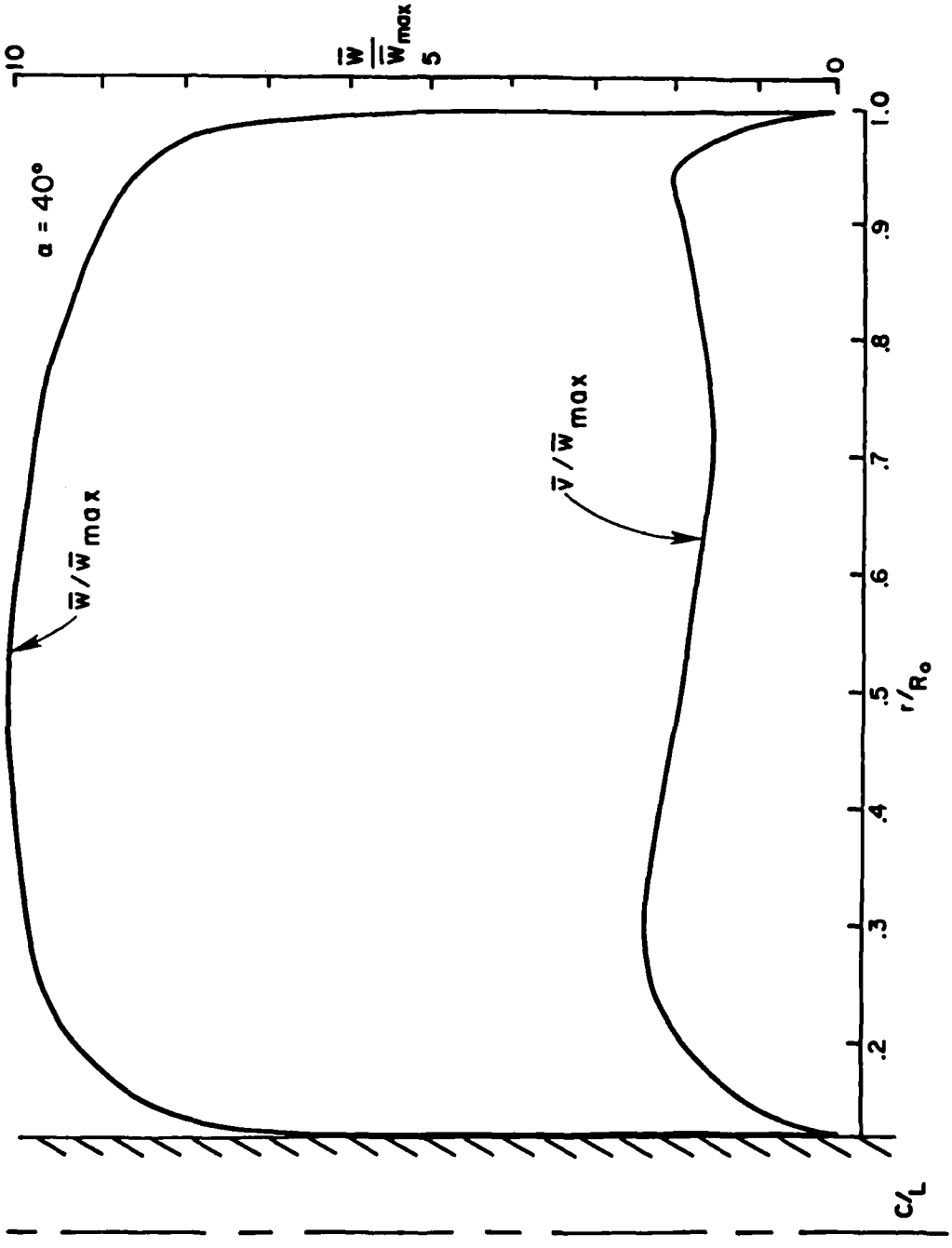
10
5
0
$\bar{w}/\bar{w}_{max}$
a = 40°
$\bar{w}/\bar{w}_{max}$
$\bar{v}/\bar{w}_{max}$
.2
.3
.4
.5
.6
.7
.8
.9
1.0
r/R_o
C_L

Figure 5(c).

$\alpha_v = 40°$, $z/D \simeq 30$ than in the previous study. These differences are due to the modification of the inlet section. The unsteadiness present without the polyurethane sheet resulted in a flow which was "stirred" more relative to the present arrangement. One of the discrepancies reported previously between the numerical modeling of this flow and the experimental observations concerned a too rapid change of the flow from vortex-like to solid body-like flow. Given the present experimental results, numerical computations using our present closure model should provide better agreement with experiment. Such numerical computations will be performed in the near future.

Turbulent Fluctuations

Turbulent velocity fluctuations were measured as a function of radius at $z/D \simeq 30$ and for three vane angle settings. The results are presented in Figure 6(a-c) where the rms fluctuations were normalized by $\bar{w}_{max}$. Again, we note that cylindrical coordinates are used where $\tilde{w}' = \sqrt{\overline{w'^2}}$, $\tilde{v}' = \sqrt{\overline{v'^2}}$, $\tilde{u}' = \sqrt{\overline{u'^2}}$ are the root mean square downstream, tangential, and radial velocity fluctuations, respectively. The $\alpha_v = 0°$ case is presented in Figure 6(a) and the behavior of the fluctuations is very typical and predictable. The $\tilde{w}'$ fluctuations receive energy directly from the deformation associated with $\bar{w}$ while $\tilde{u}'$ and $\tilde{v}'$ receive their energy indirectly through the "tendency to isotropy" terms in the equations of motion. Near the center of the annular region, all three components are approximately equal. The shape of the curves and their relative magnitudes ($\tilde{w}' > \tilde{v}' > \tilde{u}'$) agree well with the measurements of Laufer (Ref. 8). The $\alpha_v = 20°$ case is presented in Figure 6(b) where the most notable feature is the maximum in $\tilde{u}'$ near $r/R_o = 0.35$. Although $\tilde{v}'$ fluctuations now receive energy directly from the $\bar{v}$ deformation, they are still smaller than $\tilde{w}'$. This is due to the very weak tangential velocity. The $\alpha_v = 40°$ case, presented in Figure 6(c), shows that $\tilde{v}' > \tilde{w}'$ for $r/R_o < 0.40$, and this is due to the large deformation

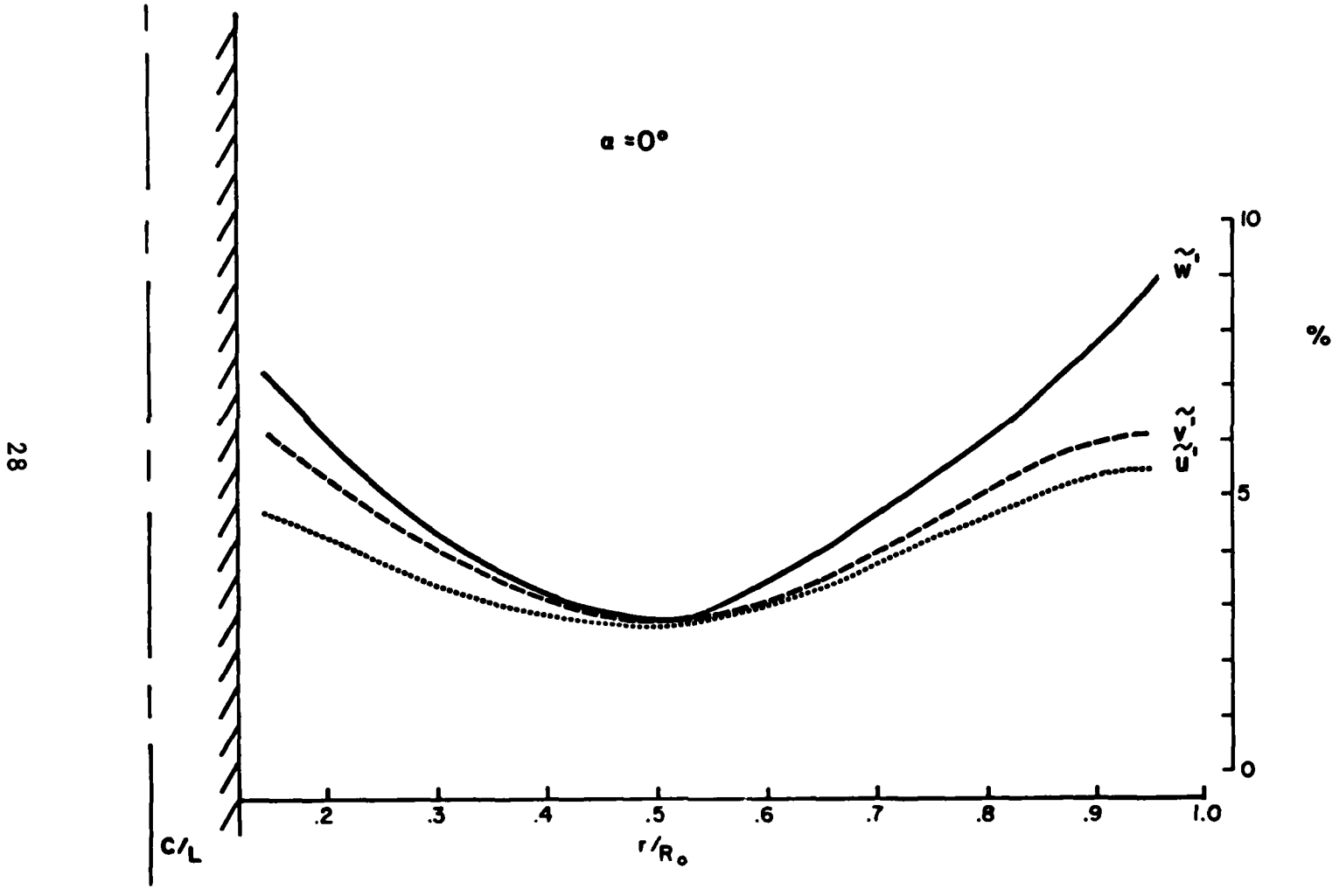

Figure 6(a).

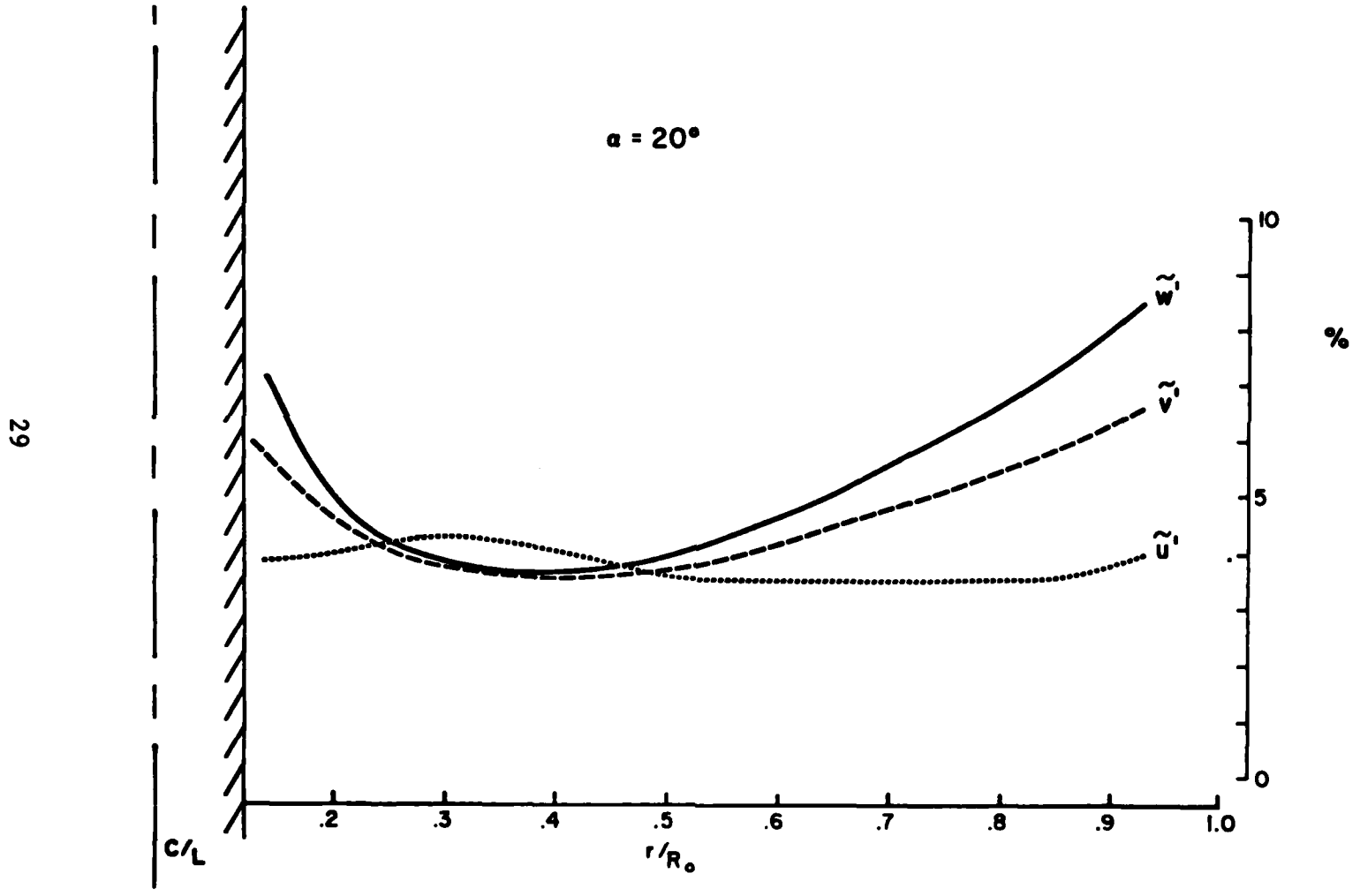

Figure 6(b).

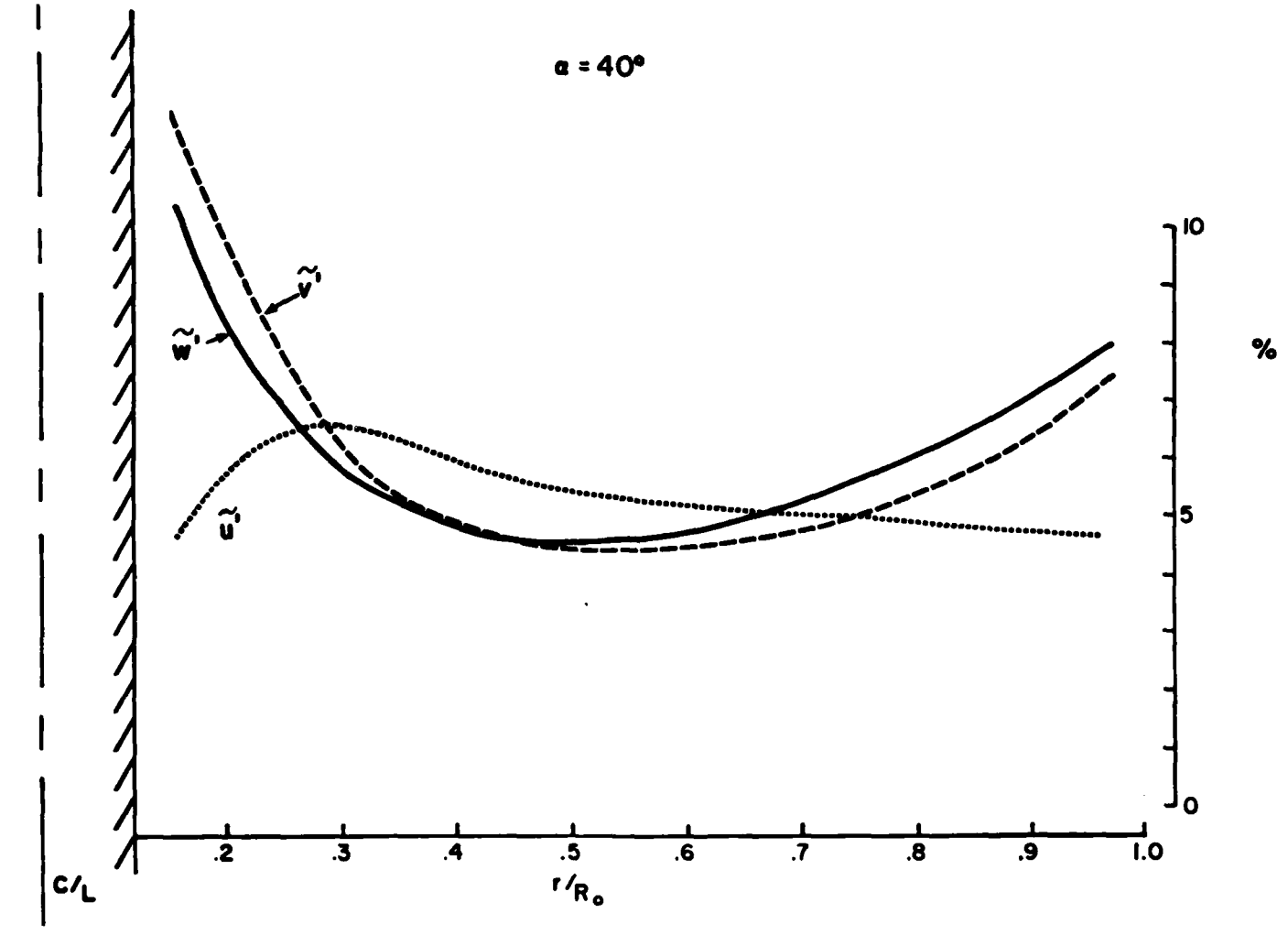

Figure 6(c).

associated with $\bar{v}$ and the direct production of $\widetilde{v}'$. As the outer wall is approached, the deformation associated with $\bar{v}$ diminishes and $\widetilde{w}' > \widetilde{v}'$. Again, a maximum value for $\widetilde{u}'$ is seen near $r/R_o = 0.30$. There are theoretical reasons to expect a region where $\widetilde{u}' > \widetilde{w}' \simeq \widetilde{v}'$ in vortex flows, but these results cannot yet support such theoretical ideas. As previously mentioned, an azimuthally propagating disturbance appears to be present in the high swirl case, and more will be said about this when power spectra are presented. At present, we do not know whether the maximum in $\widetilde{u}'$ is associated with this disturbance or represents a fundamental feature of vortex flows.

Two-Point Correlations

Two-point velocity correlations are presented in Figure 7(a-c) for the previously discussed cases. The fixed probe was positioned at $r/R_o = 0.45$ and the movable probe could be positioned from $r/R_o = 0.4575$ to 0.80, thus providing a separation distance, $\eta = \Delta r/R_o$, from 0.075 to 0.35. The data are presented for $\widetilde{w}'$, $\widetilde{v}'$, and $\widetilde{u}'$ in Figures 7(a), (b), and (c), respectively, and each figure has results from the three vane angles. The $\alpha_v = 0°$ shows the expected behavior for correlations, and the results are in fair agreement with recent two-point measurements (Ref. 9). The negative portion of the $\widetilde{w}'$ correlation is to be expected as the separation vector is perpendicular to the velocity fluctuation. Therefore, this represents a "transverse" correlation, and it is well known that such correlations have negative values at large separations. The $\alpha_v = 20°$ results show a general increase in the correlation curves, implying a greater length scale of the turbulence for this case relative to $\alpha_v = 0°$. The changes in the correlation from $\alpha_v = 0°$ to $\alpha_v = 20°$ are not very dramatic and one might

9. Hassan, H.A., Jones, B.G., and Adrian, R.J.: Measurements and Axisymmetric Model of Spatial Correlations in Turbulent Pipe Flow. AIAA Paper No. 79-1562, presented at AIAA Fluid and Plasma Dynamics Conference, 1979.

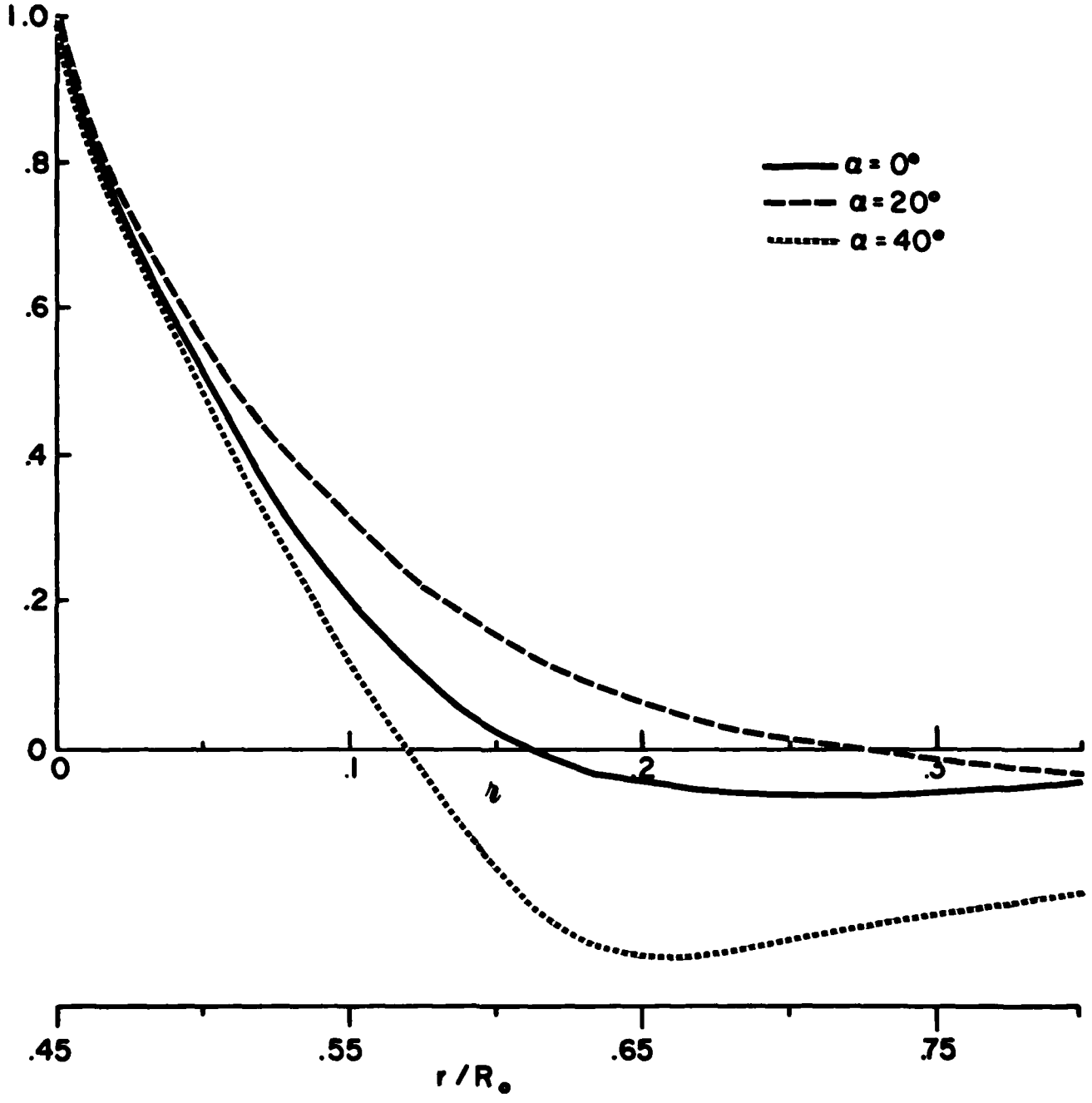

Figure 7a. Behavior of two-point correlations of axial velocity fluctuations

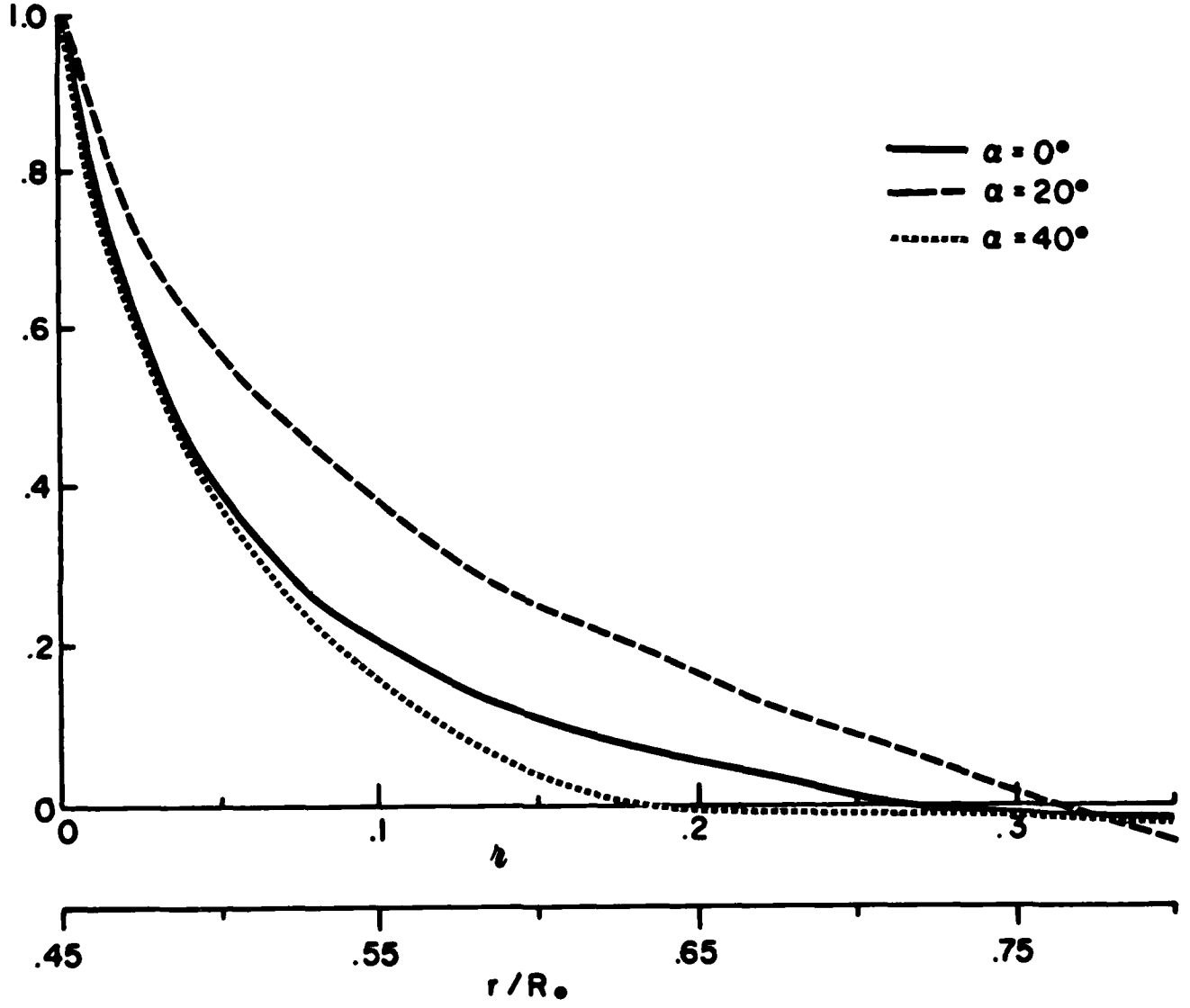

Figure 7b. Behavior of two-point correlations of tangential velocity fluctuations

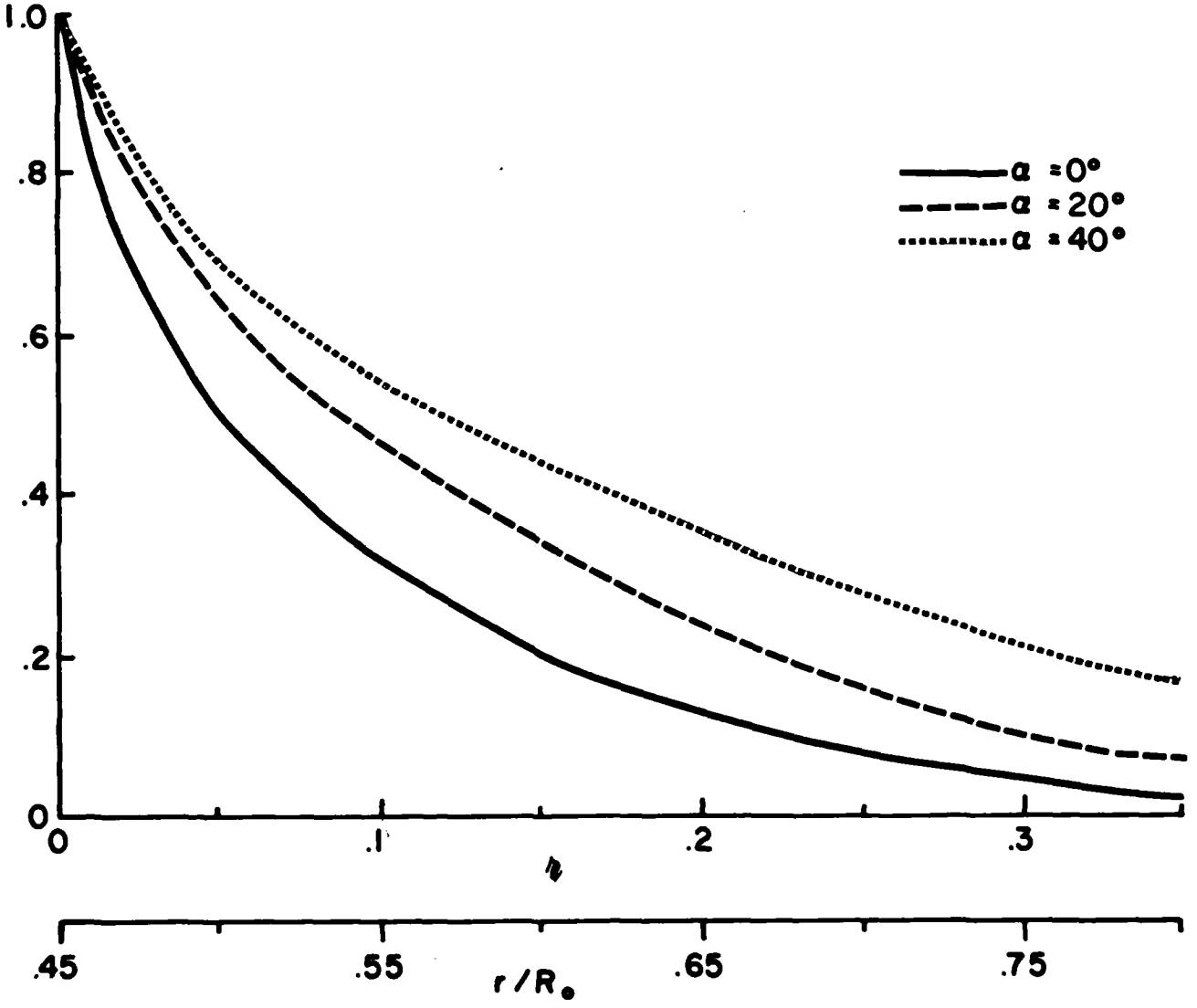

Figure 7c. Behavior of two-point correlations of radial velocity fluctuations

argue that this is because the tangential velocity is very weak. The $\alpha_v = 40°$ case does show a very dramatic change from the previous two cases. The $\widetilde{w'}$ correlation decreases more rapidly than in the previous two cases and possesses a very large negative region. The $\widetilde{v'}$ correlation also decreases more rapidly than in the previous two cases. The $\widetilde{u'}$ correlation decreases much more slowly for the $\alpha_v = 40°$ case than for the cases $\alpha_v = 0°$ and 20°. These results have just been obtained and we have yet to ascertain whether this behavior reflects some fundamental features of vortex flow or is associated with azimuthally propagating disturbances. The difference between the two swirling flow cases may well be "real" given that the deformation associated with $\bar{v}$ in the $\alpha_v = 40°$ case is far greater than in the $\alpha_v = 20°$ case.

Power Spectra

Power spectra were obtained for all three velocity components at the three vane angle settings. For the sake of brevity, we present only the $\widetilde{u'}$ spectra at $r/R_o = 0.45$ in Figure 8(a-c). The power spectra have been scaled by $\bar{w}/4\overline{u'^2}$ to yield a quantity with dimensions of length, while the frequency has been scaled by $2\pi/\bar{w}$ to yield a quantity with dimensions of inverse length. This is a standard way of treating power spectra, and originates from the fact that a turbulent length scale can be measured by extrapolating ϕ to zero frequency. The $\alpha_v = 0°$ case presented in Figure 8(a) shows a power spectra which agrees well with pipe flow results in the literature (Refs. 8, 9). The curve $k\phi$ is also plotted along with ϕ and such a curve allows one to see where the maximum energy in the spectrum occurs. The $\alpha_v = 20°$ case is presented in Figure 8(b) and one sees that the extrapolated value of ϕ to zero frequency gives a length scale greater than that obtained in the $\alpha_v = 0°$ case. This is consistent with the two-point correlation measurements which implied a greater length scale for the $\alpha_v = 20°$ case. The peak in the $k\phi$ curve occurs at a comparable position in the two cases, but a greater

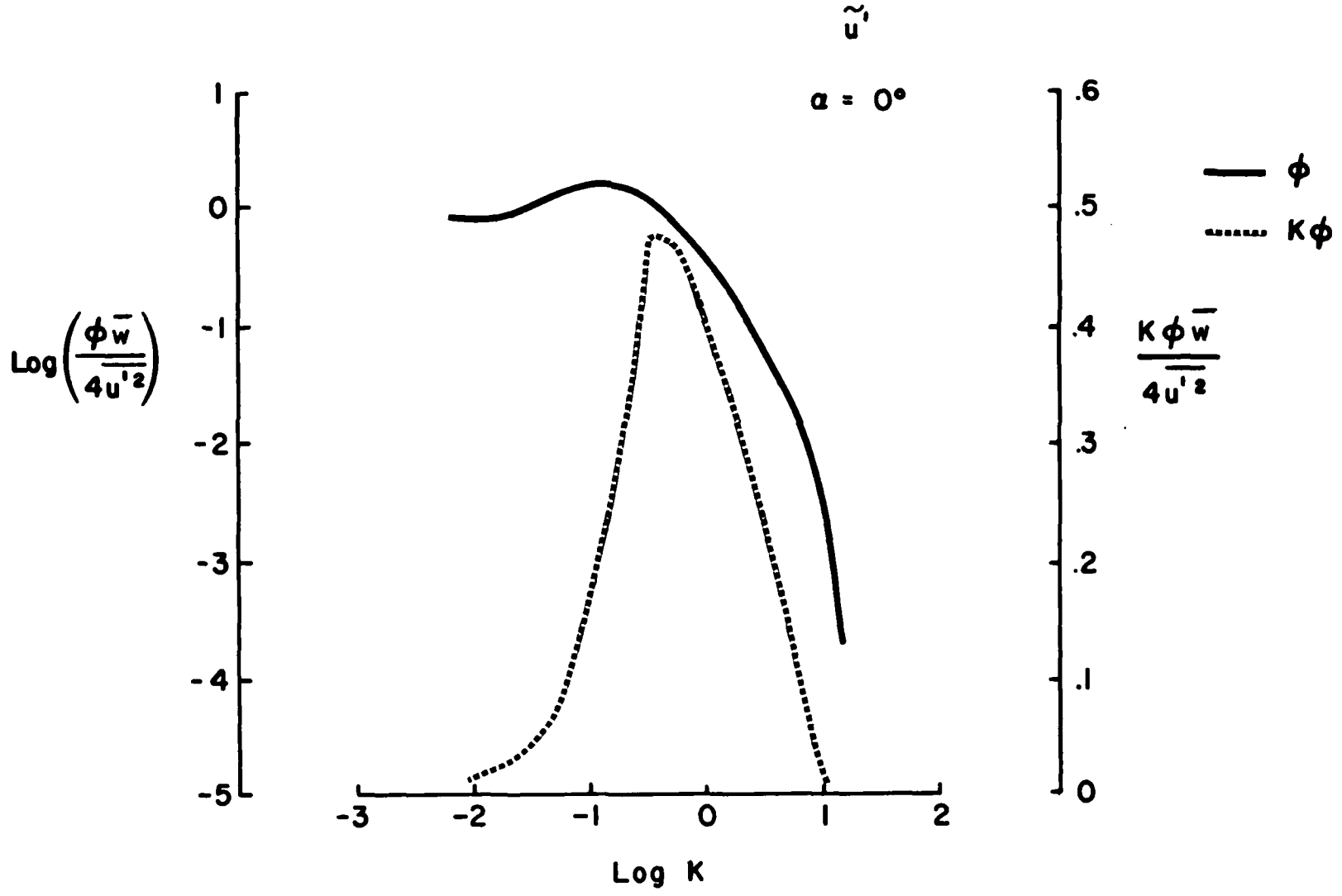
$\tilde{u}'$
α = 0°
ϕ
$K\phi$
$\text{Log}\left(\frac{\phi\bar{w}}{4\overline{u'^2}}\right)$
$\frac{K\phi\bar{w}}{4\overline{u'^2}}$
1
0
-1
-2
-3
-4
-5
.6
.5
.4
.3
.2
.1
0
-3
-2
-1
0
1
2
Log K

Figure 8a.

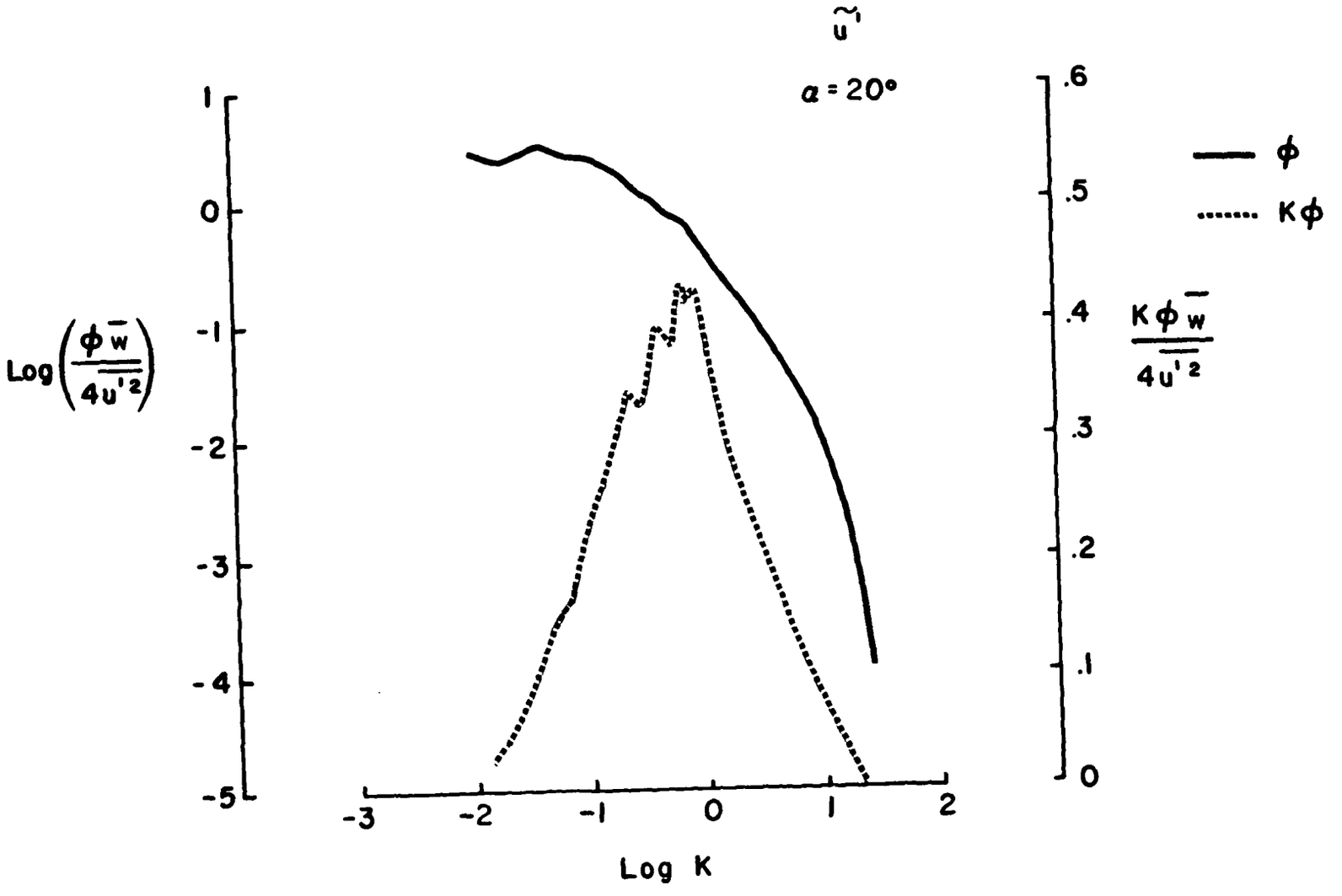

Figure 8b.

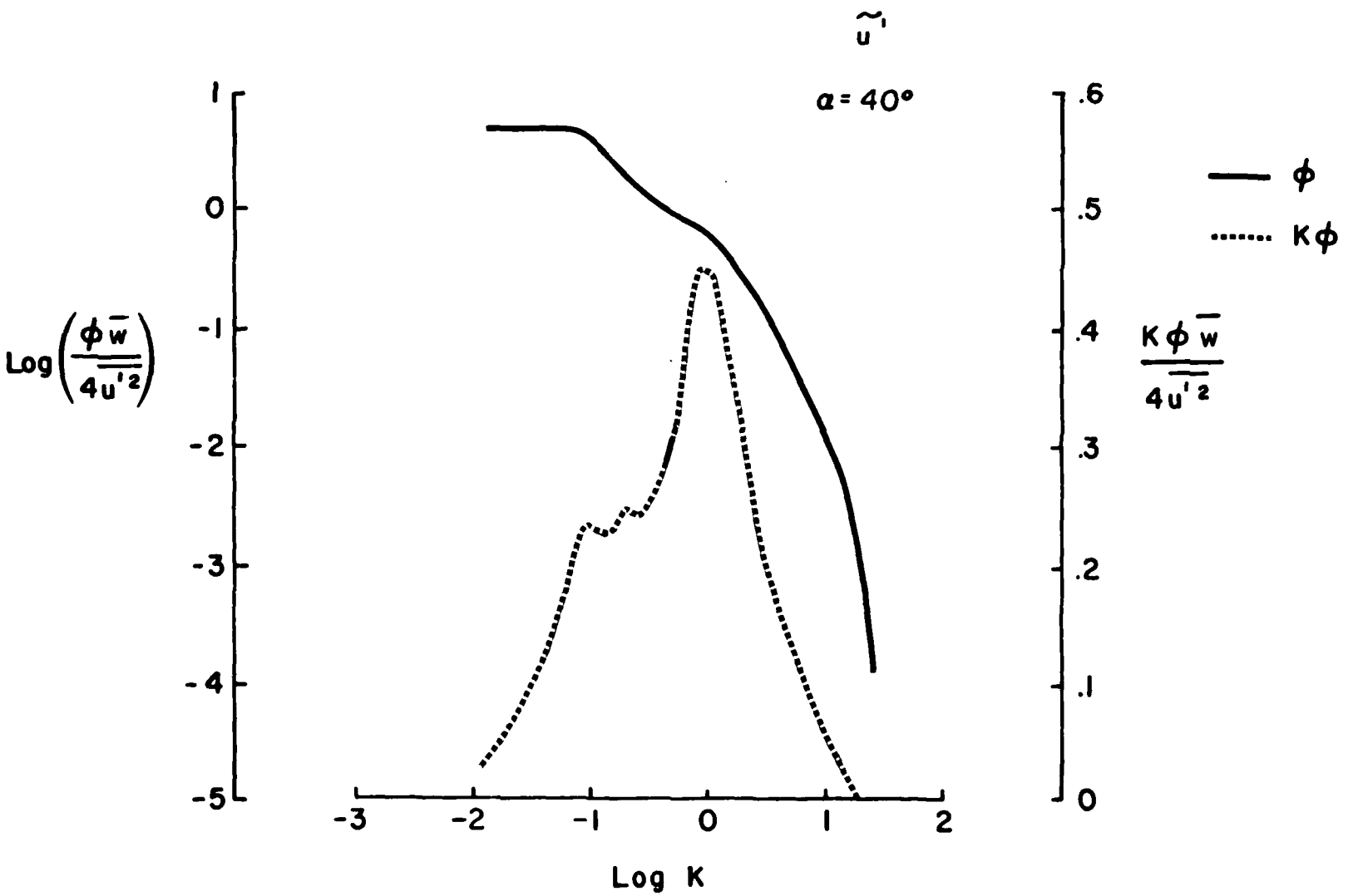
$\tilde{u}'$
$\alpha = 40°$
ϕ
$K\phi$
$\text{Log}\left(\frac{\phi\bar{w}}{4\overline{u'^2}}\right)$
$\frac{K\phi\bar{w}}{4\overline{u'^2}}$
1
0
-1
-2
-3
-4
-5
.6
.5
.4
.3
.2
.1
0
-3
-2
-1
0
1
2
Log K

Figure 8c.

contribution at low frequencies can be seen in the $\alpha_v = 20°$ case. The $\alpha_v = 40°$ case is presented in Figure 8(c) and one notices the increased energy at low frequencies. Again, the $k\phi$ curve peaks at a value similar to the previous two cases but now a sizable contribution to the energy occurs at a somewhat lower frequency. By computing a "mean flow frequency," $\bar{f} \equiv \bar{v}/2\pi r$, we find that the low frequency peak in $k\phi$ occurs at approximately $4\bar{f}$. This suggests that an azimuthally propagating disturbance with an azimuthal wave number of 4 ($m = 4$) is present. We have a number of thoughts about this disturbance. One is that we are seeing a harmonic of an $m = 1$ disturbance. Such a disturbance would arise from whatever is causing the asymmetry in the no-swirl case. Another is that we may be seeing an $m = 4$ disturbance originating from support rods in the contraction section. Alternately, we may be observing a true instability of the flowfield. Flows which have both axial and azimuthal mean velocities can be unstable to nonaxisymmetric disturbances.

Our future plans are to identify this disturbance. If the disturbance is associated with structures in the contraction section, we will attempt to eliminate them. On the other hand, if they are true instabilities, they merit study. Additional data similar to that presented here will be collected. This will enable us to measure the various turbulent length scales in the flow and have a data set which can be compared with our theoretical ideas and models of turbulent vortex flow.

4. SUMMARY

In this annual report on the status of our two-year program of theoretical and experimental studies aimed at improving computational models of turbulent flows, we have described some new methods for treating the effects of structure in turbulent flows through the use of a tensor scale equation and the two-point correlation tensor equation from which our tensor scale is derived.

We have shown that the tensor scale equation, when solved in conjunction with the Reynolds stress tensor equation, yields results that are in general agreement with the experimental results given in Reference 3 for homogeneous turbulent shear flow and for grid turbulence. The results enable one to understand the way in which homogeneous shear flows in general will reach an asymptotic state which was, we believe, just achieved at the largest times studied by Harris, Graham and Corrsin (Ref. 3).

We have shown that the kind of structure that exists in a turbulent flow, as distinct from the general scale of such structures, approaches a form determined by local equilibrium conditions rapidly, compared to changes in the mean motion. On the other hand, the scale of such structure evolves at essentially the same rate at which the overall mean motion is changing. In mathematical terms, the above statements are related, for example, to the fact that no equilibrium solution can be found for the mean scale $\Lambda = \Lambda_{ii}/3$ but equilibrium solutions can be found for the ratios Λ_{ij}/Λ .

If one considers the two-point correlation tensor equation for $R_{ij}(\vec{x},\vec{r})$, we have shown but not yet exploited that $R_{\alpha\alpha}(\vec{x},\vec{r})$ has no equilibrium solution but the deviatoric tensor $D_{ij}(\vec{x},\vec{r}) = R_{ij}(\vec{x},\vec{r}) - \frac{1}{3}\delta_{ij}R_{\alpha\alpha}(\vec{x},\vec{r})$ does have equilibrium solutions. Further, we have shown that for a differential modeling of the eddy-size rearrangement tensor, a dissipation model is deduced. It has the form that we are currently using

in our Reynolds stress closure model, which is that originally proposed by Glushko.

In addition to the above, a generalization of our single scale second-order models to better handle the problem of free convective turbulence has been developed from the general notion of a tensor scale. While this work has just been completed and has yet to be generalized for application to other flows, it has yielded very good agreement with experimental data on free convective flows.

On the experimental side, we have begun to obtain useful data from our vortex tube experiments. For the remainder of this contract, our primary emphasis will be placed on obtaining a well-documented set of data on the effect of swirl on turbulent structure in as clean an environment as we are able to produce.

5. INTERACTION WITH SCIENTIFIC COMMUNITY

Talks, Publications, and Papers in Preparation

In July of 1979, Dr. Donaldson presented some of the theoretical results outlined in this report in an invited presentation at the Second Symposium on Turbulent Shear Flows at Imperial College, London, England.

The results obtained to date are too extensive to be acceptable in a journal article of normal length. At present, we plan to publish our results in several papers that will be prepared by Drs. Sandri, Cerasoli, and Donaldson during the coming year.

Professionals Associated with Research Effort

Dr. Coleman duP. Donaldson
Dr. Guido Sandri
} Co-Principal Investigators
Dr. Carmen Cerasoli
Dr. W. Stephen Lewellen
Dr. Peter Mansfield (no longer with A.R.A.P.)
Mr. Roger D. Sullivan

Interactions

Our new tensor scale model is now up and running on the large computers at NASA/Ames, and a close liaison will continue between A.R.A.P. and the personnel at Ames who are engaged in the computation of complex turbulent flows.

The modeling of free convective flow that has been recently developed is now being used by the Navy for the calculation of the behavior of planetary boundary layers. The incorporation of the new model into atmospheric codes and the use of these codes to study atmospheric behavior is being supported by the Naval Air Systems Command.